

Interior Point Differential Dynamic Programming, Redux

Ming Xu

School of Computing
Australian National University
Canberra, ACT, Australia 2601
Email: mingda.xu@anu.edu.au

Stephen Gould

School of Computing
Australian National University
Canberra, ACT, Australia 2601
Email: stephen.gould@anu.edu.au

Iman Shames

CIICADA Lab, School of Engineering
Australian National University
Canberra, ACT, Australia 2601
Email: iman.shames@anu.edu.au

Abstract—We present IPDDP2, a structure-exploiting algorithm for solving discrete-time, finite-horizon optimal control problems (OCPs) with nonlinear constraints. Inequality constraints are handled using a primal-dual interior point formulation and step acceptance for equality constraints follows a line-search filter approach. The iterates of the algorithm are derived under the Differential Dynamic Programming (DDP) framework. A proof of local quadratic convergence of the IPDDP2 iterates is provided. Our numerical experiments evaluate IPDDP2 on over 500 OCPs derived from five different classes of robotic motion planning problems, three of which are contact-implicit trajectory optimisation problems. IPDDP2 demonstrates improvements in robustness against existing constrained DDP algorithms for contact-implicit planning, while being significantly faster than general-purpose solver IPOPT. We provide a full implementation of IPDDP2 in the Julia programming language.

I. INTRODUCTION

Discrete-time optimal control problems (OCPs) are a category of nonlinear programming problems (NLPs) that commonly arise through the discretisation of an infinite dimensional, continuous-time trajectory optimisation problem [1, 2]. OCPs are a core component of model predictive control (MPC) [3, 4], and in the context of robotics, have been used for motion planning tasks such as minimum-time quadrotor flight [5], autonomous driving [6], perceptive locomotion for legged robots [7, 8, 9, 10, 11], obstacle avoidance [12, 13, 14, 15] and manipulation [16, 17, 18, 19, 20].

OCPs have a sparsity structure that can be exploited to yield efficient, specialised numerical methods that are amenable to deployment on embedded systems [21, 22]. Of these methods, differential dynamic programming (DDP) introduced by Mayne [23, 24], holds a prominent place in the literature. Each iteration of DDP has linear time complexity with respect to the prediction horizon and has proven local quadratic and global convergence [25, 26, 27] for unconstrained OCPs. In addition, DDP maintains dynamic feasibility across iterations and provides an affine disturbance rejection state feedback policy as a byproduct of the algorithm [28, 29]. Previous works show considerable efficiency gains of DDP compared to general NLP solvers [30, 31, 32], and nonlinear MPC (NMPC) controllers using DDP have shown promising results for whole-body control for legged robots [33, 11]; in particular, the feedback policy enables a lower update rate for the controller.

Despite the promising characteristics of DDP algorithms, there has been limited success in extending DDP to handle state and/or control equality and inequality constraints. These constraints arise naturally in motion planning in robotics. Equality constraints, in particular, arise in inverse dynamics [11, 34] and *contact implicit* approaches for planning, where contact mode sequences do not need to be pre-specified a-priori [35, 36, 16, 17, 37, 38, 39]. Specific applications such as minimum-time flight for quadrotors [5], perceptive locomotion for legged robots over challenging terrain [10, 9, 11] and non-prehensile manipulation [17, 16, 19] require solving OCPs with both equality and inequality constraints.

Most existing DDP algorithms for solving OCPs with both equality and inequality constraints adopt a first-order (i.e., Gauss-Newton), *augmented Lagrangian* (AL) approach to algorithm design [30, 31, 40, 41, 42]. While these methods can be highly efficient for OCPs with high-dimensional states and/or controls (by ignoring second-order derivatives of the dynamics and constraints), we show in our experiments that they can be slow to converge for problems where strict constraint satisfaction is required. In particular, we use contact-implicit (CI) trajectory optimisation problems as an example of OCPs where constraints must be strictly satisfied, since valid contact/friction forces must satisfy various physical properties.

Motivated by this, we propose a *second-order* primal-dual interior point algorithm named Interior Point Differential Dynamic Programming v2 (IPDDP2). IPDDP2 solves OCPs with equality and inequality constraints, and builds on the IPDDP algorithm proposed in [43], which solves OCPs with inequality constraint only, to further include nonlinear *equality* constraints. We provide a formal proof of local quadratic convergence of the iterates of IPDDP2 within a neighbourhood of a solution, similar to IPDDP [43] and unconstrained DDP [27, 26]. Furthermore, we establish that a stationary point of IPDDP2 satisfies the first-order necessary conditions for optimality of the underlying OCP.

An implementation of IPDDP2 is provided in the Julia programming language¹. Our numerical experiments evaluate IPDDP2 on over 500 OCPs derived from five classes of motion planning problems with nonlinear constraints: 1) a minimum

¹<https://github.com/mingu6/InteriorPointDDP.jl>

absolute work, double integrator problem from [1], 2) a car obstacle avoidance problem, 3) a contact-implicit cart-pole swing-up task with Coulomb friction, 4) an acrobot swing-up task with joint limits enforced through a variational, contact-implicit formulation, proposed in [37] and, 5) a contact-implicit non-prehensile pushing task proposed in [17]. Our experiments indicate that IPDDP2 offers significant robustness gains and lower iteration count compared to the existing state-of-the-art constrained DDP solver ProxDDP [42], while being faster (and more amenable to embedded systems implementation) compared to the general purpose solver IPOPT [44].

Paper Outline: First, we present an overview of existing DDP algorithms in Sec. II. Next, we describe the OCPs solvable by IPDDP2 in Sec. III. We provide background on differential dynamic programming in Sec. IV. A full description of the IPDDP2 algorithm is presented in Sec. V. We present formal analysis of IPDDP2 in Sec. VI, establishing local quadratic convergence within a neighbourhood of an optimal point. Sec. VII presents the results of numerical simulations from our implementation of IPDDP2. Finally, we discuss limitations and possible extensions in Sec. VIII.

II. RELATED WORKS

In this section, we provide an overview of the literature on DDP-based algorithms for solving constrained OCPs. We note that there are other structure-exploiting solvers available [21, 22, 45], however, it is worth mentioning that these methods do not maintain dynamic feasibility across iterates and also do not provide a local feedback policy, unlike DDP.

a) Active Set Methods: Several prior works have adopted an active-set approach to DDP with constraints. Murray and Yakowitz [46] proposed a line-search algorithm which handles linear inequality constraints on states and controls, with an extension to the nonlinear case proposed by Yakowitz [47]. Tassa et al. [48] proposed a projected quasi-Newton algorithm that handles box constraints on controls. Xie et al. [32] proposed an algorithm for handling nonlinear inequality constraints using an SQP trust region approach. Unlike IPDDP2, none of these methods directly allow for nonlinear equality constraints. Furthermore, the aforementioned methods do not have any associated formal proofs of convergence.

b) Penalty Methods: Penalty methods such as the Augmented Lagrangian (AL) class of algorithms have been adapted to DDP for handling constraints. Lantoine and Russell [49] proposed an algorithm which combines an AL objective with a trust region. Howell et al. [30] (and similarly, Sleiman et al. [41]) proposed an approach based on AL, combined with an active-set projection to refine the solution. Recently, Jallet et al. [40, 42] proposed an algorithm using a primal-dual AL objective with a line-search and merit function. Mastalli et al. [11] proposed an equality constrained DDP algorithm with a line-search and merit function. However, inequality constraints are replaced with a fixed penalty function. We show that IPDDP2 provides a competitive alternative to AL-DDP methods where strict constraint satisfaction is desired, albeit at the cost of evaluating second-order dynamics and constraint

derivatives. Furthermore, unlike existing AL DDP methods, IPDDP2 admits a formal proof of convergence.

c) Interior Point Methods: The final category of constrained DDP algorithms we discuss follow an interior point formulation. Aoyama et al. [31] proposed a primal-dual interior point algorithm for solving OCPs with inequality constraints, and uses a trust region approach in the forward pass. Pavlov et al. [43] proposed primal-dual interior point DDP (IPDDP) algorithm and provided a proof of local quadratic convergence. However, equality constraints are not directly addressed by the algorithm. Recently, IPDDP was extended to include terminal state-only constraints by Aoyama et al. [50]. IPDDP2 extends IPDDP to include nonlinear equality constraints. For globalisation, IPDDP2 adopts a line-search filter approach to step acceptance, similar to IPOPT [44].

Recently, Prabhu et al. [51] proposed an interior point algorithm which addresses equality and inequality constraints based on a log-barrier formulation. In contrast, IPDDP2 adopts a primal-dual formulation, which is known to be more robust to numerical issues [52]. Furthermore, there are significant differences between Prabhu et al. [51] and IPDDP2 in the backward pass and forward pass methodology. Unlike Prabhu et al. [51], we 1) provide a proof of local quadratic convergence of IPDDP2, and 2) evaluate IPDDP2 on a diverse range of challenging benchmark problems.

III. DISCRETE-TIME OPTIMAL CONTROL VIA NONLINEAR PROGRAMMING

In this section, we will provide some background on discrete-time optimal control problems (OCPs) solvable by IPDDP2.

A. Preliminaries

We denote the i th component of a vector $v \in \mathbb{R}^n$ by $v^{(i)}$. Let $[N] = \{1, 2, \dots, N\}$ and $\|\cdot\|$ return the norm of its argument and in the absence of any subscript we mean it to be the Euclidean norm. A function $p(x) : \mathcal{X} \rightarrow \mathcal{P}$ for some sets \mathcal{X} and \mathcal{P} is defined as being $O(\|x\|^d)$ for positive integer d if there exists a scalar C such that $\|p(x)\| \leq C\|x\|^d$ for all $x \in \mathcal{X}$. A vector of ones of appropriate size is denoted by e . Denote the collection of indexed vectors $\{y_k\}_{k=t}^N$ by $y_{t:N}$ and for brevity, we use the convention $(x, u) = (x^\top, u^\top)^\top$. We use \odot to denote the element-wise product (Hadamard product). Finally, we use the following convention for derivatives: If f is a scalar valued function $f : \mathbb{R}^n \times \mathbb{R}^m \rightarrow \mathbb{R}$, then $\nabla_u f(x, u) \in \mathbb{R}^{1 \times m}$ and $\nabla_{xu}^2 f(x, u) \in \mathbb{R}^{n \times m}$. If $g : \mathbb{R}^n \times \mathbb{R}^m \rightarrow \mathbb{R}^c$ is a vector valued function, then $\nabla_x g(x, u) \in \mathbb{R}^{c \times n}$ and $\nabla_{xu}^2 g(x, u) \in \mathbb{R}^{c \times n \times m}$.

B. Problem Formulation

We consider OCPs with a finite-horizon length N , which can be expressed in the form

$$\begin{aligned} & \underset{x, u}{\text{minimise}} && J(x_{1:N}, u_{1:N}) := \sum_{t=1}^N \ell^t(x_t, u_t) \\ & \text{subject to} && x_1 = \hat{x}_1, \\ & && x_{t+1} = f^t(x_t, u_t) \quad \text{for } t \in [N-1], \\ & && c^t(x_t, u_t) = 0 \quad \text{for } t \in [N], \\ & && u_t \geq 0 \quad \text{for } t \in [N], \end{aligned} \quad (1)$$

where $x_{1:N}$ and $u_{1:N}$ are a trajectory of states and control inputs, respectively, and we assume $x_t \in \mathbb{R}^{n_x}$ and $u_t \in \mathbb{R}^{n_u}$ for all t . The running costs are denoted by $\ell^t : \mathbb{R}^{n_x} \times \mathbb{R}^{n_u} \rightarrow \mathbb{R}$ and the constraints are denoted by functions $c^t : \mathbb{R}^{n_x} \times \mathbb{R}^{n_u} \rightarrow \mathbb{R}^{n_c}$ where $n_c \leq n_u$. The mapping $f^t : \mathbb{R}^{n_x} \times \mathbb{R}^{n_u} \rightarrow \mathbb{R}^{n_x}$ captures the dynamics of the system in discrete time and \hat{x}_1 is the (known) initial state. We require that ℓ^t, f^t, c^t are twice continuously differentiable for all t .

C. Optimality Conditions

The Lagrangian of the OCP in (1) is given by

$$\begin{aligned} \mathcal{L}(\mathbf{w}, \boldsymbol{\lambda}) := & \lambda_1^\top (\hat{x}_1 - x_1) + \sum_{t=1}^N L^t(x_t, u_t, \phi_t) - z_t^\top u_t \\ & + \sum_{t=1}^{N-1} \lambda_{t+1}^\top (f^t(x_t, u_t) - x_{t+1}), \end{aligned} \quad (2)$$

where $\phi_{1:N}, z_{1:N}$ and $\boldsymbol{\lambda} := \lambda_{1:N}$ are the dual variables for the equality, inequality and dynamics constraints in (1), respectively. Furthermore, $w_t = (x_t, u_t, \phi_t, z_t)$, $\mathbf{w} := w_{1:N}$ and finally, $L^t(x_t, u_t, \phi_t) := \ell^t(x_t, u_t) + \phi_t^\top c^t(x_t, u_t)$.

The first-order optimality conditions for (1) (also known as Karush-Kuhn-Tucker (KKT) conditions), necessitate that trajectories $x_{1:N}, u_{1:N}$ can only be a local solution of (1) if there exist dual variables $\lambda_{1:N}, \phi_{1:N}$ and $z_{1:N}$ such that

$$\begin{aligned} \nabla_{x_t} \mathcal{L}(\mathbf{w}, \boldsymbol{\lambda}) = & \nabla_{x_t} L^t(x_t, u_t, \phi_t) - \lambda_t^\top \\ & + \lambda_{t+1}^\top \nabla_{x_t} f^t(x_t, u_t) = 0, \end{aligned} \quad (3a)$$

$$\begin{aligned} \nabla_{u_t} \mathcal{L}(\mathbf{w}, \boldsymbol{\lambda}) = & \nabla_{u_t} L^t(x_t, u_t, \phi_t) - z_t^\top \\ & + \lambda_{t+1}^\top \nabla_{u_t} f^t(x_t, u_t) = 0, \end{aligned} \quad (3b)$$

$$\nabla_{\lambda_t} \mathcal{L}(\mathbf{w}, \boldsymbol{\lambda}) = \begin{cases} (\hat{x}_1 - x_1)^\top = 0 & t = 1 \\ (f^{t-1}(x_{t-1}, u_{t-1}) - x_t)^\top = 0 & t > 1 \end{cases}, \quad (3c)$$

$$\nabla_{\phi_t} \mathcal{L}(\mathbf{w}, \boldsymbol{\lambda}) = c^t(x_t, u_t)^\top = 0, \quad (3d)$$

$$z_t \odot u_t = 0, \quad z_t \geq 0, \quad (3e)$$

noting that for the case $t = N$, we implicitly set $\lambda_{t+1} = 0$ since there are no dynamics constraints for step $t = N$.

Just as for any numerical algorithm based on finding a KKT point, i.e., a solution to (3), we assume throughout this paper that a suitable constraint qualification condition holds at \mathbf{x}^* and \mathbf{u}^* , e.g., linear independence of the constraint gradients. See Ch. 12 of Nocedal and Wright [53] for more details.

IV. BACKGROUND: DIFFERENTIAL DYNAMIC PROGRAMMING

In this section, we will provide some background on the Differential Dynamic Programming (DDP) class of algorithms, originally proposed by Mayne [23, 24] for unconstrained OCPs.

²This assumption is for notational simplicity only, IPDDP2 allows for time-varying state and control dimensions in general.

A. Dynamic Programming for Optimal Control

Optimal control problems are amenable to being solved using *dynamic programming* (DP), which relies on Bellman's principle of optimality [54]. Concretely, for the OCP in (1), the optimality principle at time step $t \in [N]$ yields

$$\begin{aligned} J_t^*(x_t) := & \min_{u_t} \ell^t(x_t, u_t) + J_{t+1}^*(f^t(x_t, u_t)) \\ \text{s.t. } & c^t(x_t, u_t) = 0, \quad u_t \geq 0, \end{aligned} \quad (4)$$

where J_t^* is the *value function* and boundary condition $J_{N+1}^*(x) := 0$ applies. $J_t^*(x_t)$ is the minimum cost of the sub-problem given by truncating (1) at time step t and setting the initial state to be x_t . By duality, (4) is equivalent to

$$J_t^*(x_t) := \min_{u_t} \max_{\phi_t, z_t \geq 0} L^t(x_t, u_t, \phi_t) - z_t^\top u_t + J_{t+1}^*(f^t(x_t, u_t)). \quad (5)$$

The result in (4) and (5) implies that we can decompose (1) into a sequence of sub-problems, which are solved recursively backwards in time from $t = N$. At each step of the recursion, the value function is recovered, which is then used in formulating the subsequent sub-problem.

B. Differential Dynamic Programming

The core idea used to derive the IPDDP2 algorithm (and its predecessor IPDDP [43]) is to replace the intractable value function J_t^* with a quadratic approximation \bar{V}^t . As a result, the sub-problem at time step t in (5) is replaced with

$$\min_{u_t} \max_{\phi_t, z_t \geq 0} Q^t(x_t, u_t, \phi_t, z_t), \quad (6)$$

where

$$\begin{aligned} Q^t(x_t, u_t, \phi_t, z_t) := & L^t(x_t, u_t, \phi_t) \\ & - z_t^\top u_t + V^{t+1}(f^t(x_t, u_t)). \end{aligned} \quad (7)$$

Unlike (5), the minimax sub-problem in (6) and consequently, the full DP recursion, becomes tractable.

Suppose we are given a current estimate of the primal and dual variables $\bar{\mathbf{w}}$. Each iteration of IPDDP2 has two phases, 1) the *backward pass*, which applies an approximation of a Newton step for solving (6) at $\bar{\mathbf{w}}$ to determine a local update rule and, 2) the *forward pass*, which applies the local update rule from the backward pass to update the current estimate.

V. INTERIOR POINT DIFFERENTIAL DYNAMIC PROGRAMMING

In this section, we will describe the full IPDDP2 algorithm. First, we will introduce the primal-dual interior point formulation we adopt for IPDDP2 to handle inequality constraints. Next, we introduce *backward pass* and *forward pass* phases, which together define a single iteration of the algorithm. The backward pass is applied first, computing the parameters of a local update rule using the current iterate \mathbf{w}_k . We provide a derivation of the backward pass using ideas introduced in Sec. IV. Subsequently, this update rule is used in the forward pass to update the iterates for the next iteration. The forward pass includes a step acceptance criteria based on a line-search filter method [55, 56], which enables the algorithm to converge when far away from a solution.

A. Primal-Dual Interior Point Methods

IPDDP2 is an interior point method and as such, computes approximate solutions for a sequence of *barrier sub-problems* parameterised by a sequence of positive barrier parameters $\{\mu_j\}$, with $\lim_{j \rightarrow \infty} \mu_j = 0$. A barrier sub-problem with barrier parameter $\mu > 0$ is of the form

$$\begin{aligned} & \underset{x_{1:N}, u_{1:N}}{\text{minimise}} && \sum_{t=1}^N \ell^t(x_t, u_t) - \mu \sum_{i=1}^m \ln(u_t^{(i)}) \\ & \text{subject to} && x_1 = \hat{x}_1 \\ & && x_{t+1} = f^t(x_t, u_t) \quad \text{for } t \in [N-1] \\ & && c^t(x_t, u_t) = 0 \quad \text{for } t \in [N]. \end{aligned} \quad (8)$$

This approach is equivalent to approximately solving a sequence of *perturbed KKT conditions* given by

$$\begin{aligned} \nabla_{x_t} \mathcal{L}(\mathbf{w}, \boldsymbol{\lambda}) = 0, \quad \nabla_{u_t} \mathcal{L}(\mathbf{w}, \boldsymbol{\lambda}) = 0, \quad \nabla_{\lambda_t} \mathcal{L}(\mathbf{w}, \boldsymbol{\lambda}) = 0, \\ c^t(x_t, u_t)^\top = 0, \quad z_t^* \odot u_t^* - \mu e = 0, \quad z_t^* \geq 0. \end{aligned} \quad (9)$$

We define a *perturbed KKT point* to be an iterate \mathbf{w} for which there exists $\boldsymbol{\lambda}$ such that (9) is satisfied.

Any *primal-dual method* such as IPDDP2, generates a sequence of iterates $\mathcal{I} := \{\mathbf{w}_k, \boldsymbol{\lambda}_k\}$ comprised of both primal and dual variables, where k is the iteration counter. By adjusting μ suitably as the algorithm progresses [57], the sequence \mathcal{I} converges to a solution which satisfies (3).

B. Termination Criteria

Let $w_{k,t} := (x_{k,t}, u_{k,t}, \phi_{k,t}, z_{k,t})$ be the primal and dual variables for the current iterate at time step t . The optimality error for a barrier sub-problem is defined as

$$\begin{aligned} E_\mu(\mathbf{w}_k, \boldsymbol{\lambda}_k) := \max_t \max \{ \|\nabla_{x_t} \mathcal{L}(\mathbf{w}_k, \boldsymbol{\lambda}_k)\|_\infty, \\ \|\nabla_{u_t} \mathcal{L}(\mathbf{w}_k, \boldsymbol{\lambda}_k)\|_\infty, \|c^{k,t}\|_\infty, \|z_{k,t} \odot u_{k,t} - \mu e\|_\infty \}, \end{aligned} \quad (10)$$

where $c^{k,t} := c^t(x_{k,t}, u_{k,t})$. We do not include (3c) into (10) as IPDDP2 maintains dynamic feasibility and the fixed initial state across iterates, i.e., (3c) is always satisfied exactly.

The j -th barrier sub-problem with barrier parameter μ_j is terminated when $E_{\mu_j}(\mathbf{w}_k, \boldsymbol{\lambda}_k) \leq \kappa_\epsilon \mu_j$ for some $\kappa_\epsilon > 0$. Then, the barrier parameter is updated using the rule

$$\mu_{j+1} = \max \left\{ \frac{\epsilon_{\text{tol}}}{10}, \min \left\{ \kappa_\mu \mu_j, \mu_j^{\theta_\mu} \right\} \right\}, \quad (11)$$

where $\kappa_\mu \in (0, 1)$ and $\theta_\mu \in (1, 2)$. This update rule, proposed by [57] and implemented in IPOPT [44], encourages a superlinear decrease of μ_j . We deem the algorithm to have converged if $E_0(\mathbf{w}_k, \boldsymbol{\lambda}_k) < \epsilon_{\text{tol}}$ for a user-defined optimality error tolerance $\epsilon_{\text{tol}} > 0$.

C. Backward Pass

The backward pass recursively computes the quadratic value function approximation \bar{V}^t using the current iterate \mathbf{w}_k backwards in time from $t = N$. At each step of the recursion, an update to the controls and dual variables is derived by an approximation of a Newton step applied to the KKT conditions of (6).

Preliminaries: We avoid using the iteration counter in this section for notational clarity and denote the current iterate \mathbf{w}_k by $\bar{\mathbf{w}}$. For a function $h^t \in \{\ell^t, f^t, c^t, L^t, Q^t\}$ and $y_1, y_2 \in \{x, u\}$, let $\bar{h}_{y_1}^t$ represent the partial derivative of h^t with respect to y_1 and let $\bar{h}_{y_1 y_2}^t$ represent the partial derivative of h^t with respect to y_2 followed by y_1 , evaluated at \bar{w}_t , e.g., $\bar{L}_u^t := \nabla_u L^t(\bar{x}_t, \bar{u}_t, \bar{\phi}_t)$ and $\bar{f}_{xu}^t := \nabla_{xu}^2 f^t(\bar{x}_t, \bar{u}_t)$. Let \bar{h}^t be shorthand for h^t evaluated at \bar{w}_t , e.g., $\bar{c}^t := c^t(\bar{x}_t, \bar{u}_t)$.

First, observe that \bar{V}^t can be equivalently represented by its linear and quadratic components $\bar{V}_x^t \in \mathbb{R}^{1 \times n_x}$, $\bar{V}_{xx}^t \in \mathbb{R}^{n_x \times n_x}$. Furthermore, IPDDP2 maintains an estimate of the dual variable for the dynamics constraints, denoted by $\bar{\lambda}_t$. After setting the boundary conditions

$$\bar{\lambda}_{N+1} = 0_{n_x}, \quad \bar{V}_x^{N+1} = 0_{n_x}, \quad \bar{V}_{xx}^{N+1} = 0_{n_x \times n_x}, \quad (12)$$

we proceed backwards in time from $t = N$ and alternate between computing the control and dual variable update and updating the value function approximation. Both procedures are described in the following:

a) *Computation of the Local Update:* To derive the local update, we must first introduce Newton's method applied to (6). The perturbed KKT conditions of (6) are given by

$$\begin{aligned} \nabla_{u_t} Q^t(x_t, u_t, \phi_t, z_t) = 0, \quad c^t(x_t, u_t) = 0, \\ z_t \odot u_t - \mu e = 0, \end{aligned} \quad (13)$$

to which we can apply Newton's method. Let $\delta w_t := (\delta x_t, \delta u_t, \delta \phi_t, \delta z_t)$ represent a local update to \bar{w}_t . A Newton step applied to (13) at \bar{w}_t is given by

$$\begin{bmatrix} \bar{Q}_{ux}^t & \bar{Q}_{uu}^t & A_t & -I \\ \bar{c}_x^t & A_t^\top & 0 & 0 \\ 0 & \bar{Z}_t & 0 & \bar{U}_t \end{bmatrix} \begin{bmatrix} \delta x_t \\ \delta u_t \\ \delta \phi_t \\ \delta z_t \end{bmatrix} = - \begin{bmatrix} \bar{Q}_u^t \\ \bar{c}^t \\ \bar{z}_t \odot \bar{u}_t - \mu e \end{bmatrix}, \quad (14)$$

where $A_t := [\bar{c}_u^t]^\top$, $\bar{U}_t := \text{diag}(\bar{u}_t)$, $\bar{Z}_t := \text{diag}(\bar{z}_t)$ and

$$\bar{Q}_{uu}^t := \bar{L}_{uu}^t + [\bar{f}_u^t]^\top \bar{V}_{xx}^{t+1} \bar{f}_u^t + \bar{V}_{xx}^{t+1} \cdot \bar{f}_{uu}^t, \quad (15a)$$

$$\bar{Q}_{ux}^t := \bar{L}_{ux}^t + [\bar{f}_u^t]^\top \bar{V}_{xx}^{t+1} \bar{f}_x^t + \bar{V}_{xx}^{t+1} \cdot \bar{f}_{ux}^t, \quad (15b)$$

$$\bar{Q}_{xx}^t := \bar{L}_{xx}^t + [\bar{f}_x^t]^\top \bar{V}_{xx}^{t+1} \bar{f}_x^t + \bar{V}_{xx}^{t+1} \cdot \bar{f}_{xx}^t, \quad (15c)$$

$$\bar{Q}_u^t := (\bar{L}_u^t - \bar{z}_t^\top + [\bar{V}_x^{t+1}]^\top \bar{f}_u^t)^\top. \quad (15d)$$

Furthermore, rearranging (14) yields

$$\begin{bmatrix} \bar{Q}_{uu}^t & A_t & -I \\ A_t^\top & 0 & 0 \\ \bar{Z}_t & 0 & \bar{U}_t \end{bmatrix} \begin{bmatrix} \delta u_t \\ \delta \phi_t \\ \delta z_t \end{bmatrix} = - \begin{bmatrix} \bar{Q}_u^t \\ \bar{c}^t \\ \bar{z}_t \odot \bar{u}_t - \mu e \end{bmatrix} - \begin{bmatrix} \bar{Q}_{ux}^t \\ \bar{c}_x^t \\ 0 \end{bmatrix} \delta x_t, \quad (16)$$

implying that $\delta u_t = \alpha_t + \beta_t \delta x_t$, $\delta \phi_t = \psi_t + \omega_t \delta x_t$ and $\delta z_t = \chi_t + \zeta_t \delta x_t$ for some parameters $\alpha_t, \beta_t, \psi_t, \omega_t, \chi_t$ and ζ_t .

IPDDP2 applies an approximation to (16) in determining the update rule parameters, i.e., the parameters must satisfy

$$\underbrace{\begin{bmatrix} H_t & A_t & -I \\ A_t^\top & 0 & 0 \\ \bar{Z}_t & 0 & \bar{U}_t \end{bmatrix}}_{K_t} \begin{bmatrix} \alpha_t & \beta_t \\ \psi_t & \omega_t \\ \chi_t & \zeta_t \end{bmatrix} = - \begin{bmatrix} \bar{Q}_u^t & B_t \\ \bar{c}^t & \bar{c}_x^t \\ \bar{z}_t \odot \bar{u}_t - \mu e & 0 \end{bmatrix}, \quad (17)$$

where

$$H_t := \bar{L}_{uu}^t + [\bar{f}_u^t]^\top \bar{V}_{xx}^{t+1} \bar{f}_u^t + \bar{\lambda}_{t+1} \cdot \bar{f}_{uu}^t, \quad (18a)$$

$$B_t := \bar{L}_{ux}^t + [\bar{f}_u^t]^\top \bar{V}_{xx}^{t+1} \bar{f}_x^t + \bar{\lambda}_{t+1} \cdot \bar{f}_{ux}^t, \quad (18b)$$

$$C_t := \bar{L}_{xx}^t + [\bar{f}_x^t]^\top \bar{V}_{xx}^{t+1} \bar{f}_x^t + \bar{\lambda}_{t+1} \cdot \bar{f}_{xx}^t, \quad (18c)$$

and \cdot denotes a tensor contraction along the first dimension.

Comparing (15) to (18), H_t, B_t and C_t differ from $\bar{Q}_{uu}^t, \bar{Q}_{ux}^t$ and \bar{Q}_{xx}^t , respectively, only by the vector used in the tensor contraction ($\bar{\lambda}_{t+1}$ instead of \bar{V}_x^{t+1}). This difference is essential in establishing the local convergence result in Sec. VI.

Implementation Details: In our implementation of IPDDP2, we avoid solving (17) directly and equivalently, solve the symmetric, condensed iteration matrix derived through eliminating the last block row, i.e.,

$$\underbrace{\begin{bmatrix} H_t + \Sigma_t & A_t \\ A_t^\top & 0 \end{bmatrix}}_{K'_t} \begin{bmatrix} \alpha_t & \beta_t \\ \psi_t & \omega_t \end{bmatrix} = - \begin{bmatrix} \hat{Q}_u^t & B_t \\ \bar{c}^t & \bar{c}_x^t \end{bmatrix}, \quad (19)$$

where $\Sigma_t := \bar{U}_t^{-1} \bar{Z}_t$ and

$$\hat{Q}_u^t := (\bar{L}_u^t - \mu e^\top \bar{U}_t^{-1} + [\bar{V}_x^{t+1}]^\top \bar{f}_u^t)^\top. \quad (20)$$

Parameters χ_t and ζ_t are subsequently recovered using

$$\chi_t = \mu \bar{U}_t^{-1} e - \bar{z}_t - \Sigma_t \alpha_t, \quad \zeta_t = -\Sigma_t \beta_t. \quad (21)$$

Furthermore, motivated by the global convergence proof of the line-search filter algorithm in [55], we desire that $H_t + \Sigma_t$ be positive definite on the null-space of A_t for all t at each iteration. A sufficient condition for this requirement is for K'_t to have an inertia of $(n_u, n_c, 0)$ for all t , where the inertia is the number of positive, negative and zero eigenvalues, respectively.

To enforce this condition on the inertia, we implement an *inertia correction heuristic* which replaces (19) with

$$\underbrace{\begin{bmatrix} H_t + \Sigma_t + \delta_w I & A_t \\ A_t^\top & -\delta_c I \end{bmatrix}}_{K''_t} \begin{bmatrix} \alpha_t & \beta_t \\ \psi_t & \omega_t \end{bmatrix} = - \begin{bmatrix} \hat{Q}_u^t & B_t \\ \bar{c}^t & \bar{c}_x^t \end{bmatrix}, \quad (22)$$

where $\delta_w, \delta_c \geq 0$ independent of t , are chosen so that K''_t has the desired inertia. We restart the backward pass, after updating δ_w, δ_c according to Alg. IC in [44], if the inertia condition fails to hold for any t . We use a Bunch-Kaufman LDLT factorisation [58] with rook pivoting [59] to simultaneously solve (19) and recover its inertia.

b) Updating the Value Function Approximation: After computing the update rule parameters, the value function approximation and $\bar{\lambda}$ are updated according to the rule

$$\bar{V}_x^t := (\bar{L}_x^t + [\bar{V}_x^{t+1}]^\top \bar{f}_x^t)^\top + \beta_t^\top \hat{Q}_u^t + \omega_t^\top \bar{c}_x^t, \quad (23a)$$

$$\bar{\lambda}_x^t := (\bar{L}_x^t + \bar{\lambda}_{t+1}^\top \bar{f}_x^t)^\top, \quad \bar{V}_{xx}^t := C_t + \beta_t^\top B_t + \omega_t^\top \bar{c}_x^t. \quad (23b)$$

The time step is then decremented, i.e., $t \leftarrow t - 1$ and the computation of the update rule parameters (a) repeated.

D. Forward Pass

The IPDDP2 forward pass applies a backtracking line-search procedure to generate trial points for the next iterate, using the update rule established from the backward pass. Given a step size $\gamma \in (0, 1]$, a corresponding trial point is calculated by applying the formula

$$\begin{aligned} x_{t+1}^+ &= f^t(x_t^+, u_t^+(\gamma)), \quad x_1^+ = \hat{x}_1, \\ u_t^+(\gamma) &= \bar{u}_t + \gamma \alpha_t + \beta_t(x_t^+ - \bar{x}_t), \\ \phi_t^+(\gamma) &= \bar{\phi}_t + \gamma \psi_t + \omega_t(x_t^+ - \bar{x}_t), \\ z_t^+(\gamma) &= \bar{z}_t + \gamma \chi_t + \zeta_t(x_t^+ - \bar{x}_t), \end{aligned} \quad (24)$$

forward in time starting from $t = 1$. A trial point $\mathbf{w}^+(\gamma)$, where $\mathbf{w}_t^+(\gamma) := (x_t^+, u_t^+(\gamma), \phi_t^+(\gamma), z_t^+(\gamma))$ is accepted as the next iterate if certain step acceptance criteria, to be described in the remainder of this section are satisfied. After a trial point is accepted, the algorithm proceeds to the next iteration.

The step size corresponding to the accepted trial point, denoted by $\bar{\gamma}$, is determined using a backtracking line search procedure which explores a sequence of step sizes starting from $\gamma = 1$, setting $\gamma \leftarrow \frac{1}{2}\gamma$ if $\mathbf{w}^+(\gamma)$ fails to satisfy the step acceptance criteria.

a) Fraction-to-the-Boundary Criteria: The first step acceptance criterion is an element-wise *fraction-to-the-boundary* condition, where a trial point corresponding to step size γ must satisfy

$$u_t^+(\gamma) \geq (1 - \tau)u_t, \quad z_t^+(\gamma) \geq (1 - \tau)z_t \quad \text{for all } t, \quad (25)$$

and $\tau = \max\{\tau_{\min}, 1 - \mu\}$ for some $\tau_{\min} > 0$. Condition (25) prevents iterates from reaching the constraint boundaries too quickly and is commonly found in interior point methods, e.g., [44, 43, 53].

b) Line-Search Filter Criteria: The next step acceptance criterion requires that a trial point corresponding to step size γ must yield a sufficient decrease in *either* the Lagrangian of the barrier sub-problem in (8) or the constraint violation when compared to the current iterate. Concretely, let the constraint violation and Lagrangian for the barrier problem (8) be given by $\theta(\mathbf{w})$ and $\mathcal{L}_\mu(\mathbf{w})$, respectively, where

$$\theta(\mathbf{w}) := \sum_{t=1}^N \|c^t(x_t, u_t)\|_1, \quad (26a)$$

$$\mathcal{L}_\mu(\mathbf{w}) := \sum_{t=1}^N L^t(x_t, u_t, \phi_t) - \mu \sum_{i=1}^m \ln(u_t^{(i)}). \quad (26b)$$

We adopt the sufficient decrease condition given by

$$\theta(\mathbf{w}^+(\gamma)) \leq (1 - \gamma_\theta)\theta(\bar{\mathbf{w}}) \quad \text{or} \quad (27a)$$

$$\mathcal{L}_\mu(\mathbf{w}^+(\gamma)) \leq \mathcal{L}_\mu(\bar{\mathbf{w}}) - \gamma_\mathcal{L}\theta(\bar{\mathbf{w}}), \quad (27b)$$

for prescribed constants $\gamma_\theta, \gamma_\mathcal{L} \in (0, 1)$. However, as noted in [55], accepting steps solely based on (27) could result in convergence to a feasible, but sub-optimal point. As a result, (27) is replaced by enforcing a sufficient decrease in the

Lagrangian of the barrier sub-problem if both $\theta(\bar{\mathbf{w}}) < \theta_{\min}$ for some small θ_{\min} and the *switching condition*

$$m(\gamma) < 0 \quad \text{and} \quad [-m(\gamma)]^{s_{\mathcal{L}}} \gamma^{1-s_{\mathcal{L}}} > \delta[\theta(\bar{\mathbf{w}})]^{s_{\theta}} \quad (28)$$

holds, where $\delta > 0$, $s_{\theta} > 1$, $s_{\mathcal{L}} \geq 1$ are constants and $m(\gamma)$ is a model of the Lagrangian of the barrier sub-problem given by

$$m(\gamma) := \sum_{t=1}^N \gamma \left(\alpha_t^{\top} \hat{Q}_u^t + \psi_t^{\top} \bar{c}^t \right). \quad (29)$$

The sufficient decrease condition which must hold if (28) holds is analogous to the Armijo condition, and is given by

$$\mathcal{L}_{\mu}(\mathbf{w}^+(\gamma)) \leq \mathcal{L}_{\mu}(\bar{\mathbf{w}}) + \eta_{\mathcal{L}} m(\gamma) \quad (30)$$

for some small $\eta_{\mathcal{L}} > 0^3$. Accepted iterates which satisfy (28) and (30) are called \mathcal{L} -type iterations [44].

Accepting steps solely based on the above method may cause cycling, where iterates alternate between decreasing the objective and the constraint violation while increasing the other. To address this, IPDDP2 maintains a *filter*, denoted by $\mathcal{F} \subseteq \{(\theta, \mathcal{L}) \in \mathbb{R}^2 : \theta \geq 0\}$. The set \mathcal{F} defines a ‘‘taboo’’ region for iterates, and a trial point is rejected if it is not acceptable to the filter, i.e., $(\theta^+, \mathcal{L}^+) \in \mathcal{F}$.

We follow the approach described in [44], and initialise the filter with $\mathcal{F} = \{(\theta, \mathcal{L}) \in \mathbb{R}^2 : \theta \geq \theta_{\max}\}$ for some θ_{\max} . For each iteration, after a trial point $\mathbf{w}^+(\gamma)$ is accepted, the filter is augmented if either (28) or (30) do not hold, using

$$\mathcal{F}^+ := \mathcal{F} \cup \left\{ (\theta, \mathcal{L}) \in \mathbb{R}^2 : \theta \geq (1 - \gamma_{\theta})\theta(\bar{\mathbf{w}}), \right. \\ \left. \mathcal{L} \geq \mathcal{L}_{\mu}(\bar{\mathbf{w}}) - \gamma_{\mathcal{L}}\theta(\bar{\mathbf{w}}) \right\}. \quad (31)$$

E. Complete IPDDP2 Algorithm

Solving a barrier sub-problem involves alternating between the backward and forward passes described in Sec. V-C and V-D. The complete IPDDP2 algorithm is presented in Alg. 1.

Algorithm 1.

Given: Starting point \mathbf{w}_0 ; $\epsilon_{\text{tol}}, \epsilon_{\min} > 0$; $\theta_{\max} \in (0, \infty]$; $\gamma_{\theta}, \gamma_{\mathcal{L}} \in (0, 1)$; $\delta > 0$; $\kappa_{\epsilon}, \kappa_{\mu} > 0$; $s_{\theta} > 1$; $s_{\mathcal{L}} \geq 1$; $\tau_{\min} > 0$; $\eta_{\mathcal{L}} \in (0, \frac{1}{2})$; $\text{max_iters} > 0$; $\mu_{\text{init}} > 0$; $\gamma^{\min} > 0$; $\mu_{\text{init}} > 0$.

1. *Initialise.* Initialise the iteration counter $k \leftarrow 0$, barrier problem counter $j \leftarrow 0$, $\mu_j = \mu_{\text{init}}$ and filter $\mathcal{F}_0 := \{(\theta, \mathcal{L}) \in \mathbb{R}^2 : \theta \geq \theta_{\max}\}$.
2. *Backward pass.* Compute update rule parameters and λ_k by setting (12), time counter $t \leftarrow N$.
 - 2.1. If $t = 0$, go to step 3.
 - 2.2. Solve for $\alpha_{k,t}, \beta_{k,t}, \psi_{k,t}, \omega_{k,t}, \chi_{k,t}$ and $\zeta_{k,t}$ using (22). If the matrix in (22) is too ill conditioned, terminate the algorithm.
 - 2.3. Update $V_x^{k,t}, V_{xx}^{k,t}, \lambda_{k,t}$ using (23).
 - 2.4. Set $t \leftarrow t - 1$ and go to 2.1.
3. *Check convergence of overall problem.* If $E_0(\mathbf{w}_k, \lambda_k) < \epsilon_{\text{tol}}$ then STOP (converged). If $k = \text{max_iters}$ then STOP (not converged).

³Global convergence was established for unconstrained DDP by [25] using this condition along with a backtracking line-search.

4. *Check convergence of barrier problem.* If $E_{\mu_j}(\mathbf{w}_k, \lambda_k) < \kappa_{\epsilon} \mu_j$ then:

- 4.1. Compute μ_{j+1} and τ_{j+1} from (11) and (25).
- 4.2. Re-initialise the filter $\mathcal{F}_k := \{(\theta, \mathcal{L}) \in \mathbb{R}^2 : \theta \geq \theta_{\max}\}$.
- 4.3. If $k = 0$, repeat step 4., otherwise continue at 5.

5. *Backtracking line search.*

- 5.1. *Initialise line search.* Set $\gamma_{k,0} = 1$ and $l \leftarrow 0$.
- 5.2. *Compute new trial point.* If the trial step size $\gamma_{k,l}$ becomes too small, i.e., $\gamma_{k,l} < \gamma^{\min}$, terminate the algorithm. Otherwise, compute the new trial point $\mathbf{w}^+(\gamma_{k,l})$ using the forward pass, i.e., (24).
- 5.3. *Check acceptability to the filter.* If (27) does not hold, reject the trial step size and go to step 6.
- 5.4. *Check sufficient decrease with respect to the current iterate.*
 - 5.4.1. *Case I:* $\gamma_{k,l}$ is a \mathcal{L} -step size (i.e., (28) holds). If the Armijo condition (30) holds, accept the trial step and go to step 7. Otherwise, go to step 6.
 - 5.4.2. *Case II:* $\gamma_{k,l}$ is not a \mathcal{L} -step size, (i.e., (28) is not satisfied): If (27) holds, accept the trial step and go to step 7. Otherwise, go to step 6.
6. *Choose new trial step size.* Choose $\gamma_{k,l+1} = \frac{1}{2} \gamma_{k,l}$, set $l \leftarrow l + 1$ and go back to step 5.2.
7. *Accept trial point.* Set $\gamma_k := \gamma_{k,l}$ and $\mathbf{w}_{k+1} := \mathbf{w}_k^+(\gamma_k)$.
8. *Augment filter if necessary.* If k is not a \mathcal{L} -type iteration, augment the filter using (31); otherwise leave the filter unchanged, i.e., set $\mathcal{F}_{k+1} := \mathcal{F}_k$.
9. *Continue with next iteration.* Increase the iteration counter $k \leftarrow k + 1$ and go back to step 2.

VI. FORMAL ANALYSIS OF IPDDP2

In this section, we formally analyse the convergence properties of a simplified version IPDDP2 algorithm. Concretely, we consider a simplified IPDDP2 algorithm comprised of alternating between the backward and forward pass phases defined in Sec. V-C and V-D for a *fixed* barrier parameter μ . To simplify the analysis further, we assume that if the current iterate is sufficiently close to a perturbed KKT point, then the step acceptance criteria detailed in Sec. V-D accepts full steps of size $\gamma = 1$ for all subsequent iterations.

We establish two results, 1) that an iterate \mathbf{w} is a perturbed KKT point if and only if it is also a fixed point of the simplified IPDDP2 algorithm and, 2) that when the current iterate is sufficiently close to a perturbed KKT point, then the simplified IPDDP2 algorithm converges to the perturbed KKT point at a quadratic rate. First, we present some additional assumptions made throughout this section.

Assumptions 1. We assume for all $t \in [N]$ there exists an open convex neighbourhood \mathcal{N}_t containing w_t^* and the current iterate \bar{w}_t , such that for all $w_t \in \mathcal{N}_t$ and all $t \in [N]$ and

- (1A) functions ℓ^t, f^t, c^t and their first derivatives are Lipschitz continuously differentiable;
- (1B) $\hat{H}_t := H_t + \Sigma_t$ is non-singular with bounded inverse;
- (1C) the minimum singular value of A_t is uniformly bounded away from zero; and

(1D) \hat{H}_t is positive definite in the null space of A_t .

Assumption (1D) ensures that no inertia correction is applied in the backward pass and furthermore, that the backward pass is well-defined by non-singularity of the iteration matrix K_t .

A. Stationarity of IPDDP2 at a KKT Point

For our first result, we show an iterate generated by the IPDDP2 algorithm is a perturbed KKT point if and only if it is a fixed point of the IPDDP2 algorithm. We define a fixed point of IPDDP2 to be an iterate $\bar{\mathbf{w}}$ which is not updated after applying the IPDDP2 forward pass, i.e., $\alpha_t = 0$, $\psi_t = 0$ and $\chi_t = 0$ for all $t \in [N]$. This holds if and only if $\bar{Q}_u^t = 0$, $\bar{c}^t = 0$ and $\bar{u}_t \odot \bar{z}_t = \mu e$, i.e., the block left column on the right side of (17) is zero, since K_t is non-singular.

Theorem 1. *Let $\bar{\mathbf{w}}$ be a strictly primal-dual feasible point which satisfies $\bar{u}_t > 0$, $\bar{z}_t > 0$, $\bar{x}_{t+1} = f^t(\bar{x}_t, \bar{u}_t)$, $\bar{x}_1 = \hat{x}_1$. Then $\bar{\mathbf{w}}$ is a stationary point of IPDDP2 if and only if it is also a perturbed KKT point.*

Proof: Suppose $\bar{\mathbf{w}}$ is a stationary point of IPDDP2. Then $\bar{Q}_u^t = 0$, $\bar{c}^t = 0$ and $\bar{z}_t \odot \bar{u}_t - \mu e = 0$. By (20) and $\bar{z}_t = \mu \bar{U}_t^{-1} e$, it follows that $\bar{Q}_u^t = 0$. Since $\bar{Q}_u^t = 0$ and $\bar{c}^t = 0$, by (23a) $\bar{V}_x^t = \bar{\lambda}_t$ for all $t \in [N]$. By (15d) $\nabla_{u_t} \mathcal{L}(\bar{\mathbf{w}}, \bar{\lambda}) = \bar{L}_u^t - \bar{z}_t^\top + \bar{\lambda}_{t+1}^\top \bar{f}_u^t = 0$. Substituting the update rule for $\bar{\lambda}_t$ from (23) into (3a) yields $\nabla_{x_t} \mathcal{L}(\bar{\mathbf{w}}, \bar{\lambda}) = 0$. The remaining KKT conditions in (9) are satisfied by assumption.

Now suppose that $\bar{\mathbf{w}}$ satisfies the perturbed KKT conditions (9). Then $\nabla_{u_t} \mathcal{L}(\bar{\mathbf{w}}, \bar{\lambda}) = \bar{L}_u^t - \bar{z}_t^\top + \bar{\lambda}_{t+1}^\top \bar{f}_u^t = 0$, $\nabla_{x_t} \mathcal{L}(\bar{\mathbf{w}}, \bar{\lambda}) = \bar{L}_x^t - \bar{\lambda}_t^\top + \bar{\lambda}_{t+1}^\top \bar{f}_x^t = 0$, $\bar{z}_t \odot \bar{u}_t - \mu e = 0$ and $\bar{c}^t = 0$. By (23a) and $\bar{c}^N = 0$, $\bar{V}_x^N = \bar{\lambda}_N$. Since $\bar{z}_N = \mu \bar{U}_N^{-1} e$, by (20), $\bar{Q}_u^N = 0$ and thus by (23) and $\bar{c}^{N-1} = 0$, $\bar{V}_x^{N-1} = \bar{\lambda}_{N-1}$. Proceeding backwards in time yields $\bar{Q}_u^t = 0$ and $\bar{V}_x^t = \bar{\lambda}_t$ for all $t \in [N]$. We conclude that since $\bar{Q}_u^t = \bar{Q}_u^t = 0$, $\bar{c}^t = 0$ and $\bar{u}_t \odot \bar{z}_t - \mu e = 0$, $\bar{\mathbf{w}}$ is a stationary point of IPDDP2. ■

B. Local Quadratic Convergence of IPDDP2

We now establish the local quadratic convergence properties of IPDDP2. Before we present the main result, we establish a preliminary result regarding the value function approximation \bar{V}^t . In the remainder of this section, denote the current and updated iterates by $\bar{\mathbf{w}}$ and \mathbf{w}^+ , respectively and denote a point which satisfies the perturbed KKT conditions by \mathbf{w}^* .

Proposition 1. *Let $\lambda^{N+1}(\cdot) = 0$ and for $t \in [N]$, let*

$$\lambda^t(w_{t:N}) := \nabla_{x_t} L^t(x_t, u_t, \phi_t)^\top + \nabla_{x_t} f^t(x_t, u_t)^\top \lambda^{t+1}(w_{t+1:N}) \quad (32)$$

and $\lambda^t(\bar{w}_{t:N}) = \bar{\lambda}_t$. Under Assumptions 1,

$$\lambda^t(w_{t:N}^*) = \bar{V}_x^t + \bar{V}_{xx}^t (x_t^* - \bar{x}_t) + O(\|\bar{\mathbf{w}} - \mathbf{w}^*\|^2). \quad (33)$$

Proof: We proceed with an inductive argument. The base case of $t = N+1$ holds since $\lambda^{N+1} = 0$, and by (12), $\bar{V}_x^{N+1} = 0$ and $\bar{V}_{xx}^{N+1} = 0$. Now suppose (33) holds for step $t+1$ for some $t \in [N]$. By Assumption (1A), we can apply

Taylor's theorem to the dynamics, constraints and perturbed complementary slackness conditions, yielding

$$x_{t+1}^* = \bar{x}_{t+1} + \bar{f}_x^t(x_t^* - \bar{x}_t) + \bar{f}_u^t(u_t^* - \bar{u}_t) + O(\|\bar{w}_t - w_t^*\|^2), \quad (34)$$

$$0 = c^t(x_t^*, u_t^*) = \bar{c}^t + A_t^\top (u_t^* - \bar{u}_t) + \bar{c}_x^t (x_t^* - \bar{x}_t) + O(\|\bar{\mathbf{w}} - \mathbf{w}^*\|^2), \quad (35)$$

$$\mu e = u_t^* \odot z_t^* = \bar{U}_t \bar{z}_t + \bar{Z}_t (u_t^* - \bar{u}_t) + \bar{U}_t (z_t^* - \bar{z}_t) + O(\|\bar{\mathbf{w}} - \mathbf{w}^*\|^2), \quad (36)$$

respectively. In addition, multiplying (36) by \bar{U}_t^{-1} and rearranging for z_t^* yields

$$z_t^* = \mu \bar{U}_t^{-1} e - \Sigma_t (u_t^* - \bar{u}_t) + O(\|\bar{\mathbf{w}} - \mathbf{w}^*\|^2). \quad (37)$$

By Assumption (1A), the derivatives of λ^t exist and are bounded locally, therefore, we can apply Taylor's theorem to λ^t and use (33) to yield

$$\begin{aligned} \lambda^t(w_{t:N}^*) &= \lambda^t(\bar{w}_{t:N}) + \nabla_{w_t} \lambda^t(\bar{w}_{t:N})(w_t^* - \bar{w}_t) \\ &\quad + \nabla_{w_{t+1:N}} \lambda^t(\bar{w}_{t:N})(w_{t+1:N}^* - \bar{w}_{t+1:N}) \\ &\quad + O(\|\bar{\mathbf{w}} - \mathbf{w}^*\|^2) \\ &\stackrel{(32)}{=} [\bar{L}_x^t]^\top + \nabla_{w_t} \lambda^t(\bar{w}_{t:N})(w_t^* - \bar{w}_t) + [\bar{f}_x^t]^\top (\\ &\quad \nabla_{w_{t+1:N}} \lambda^{t+1}(\bar{w}_{t+1:N})(w_{t+1:N}^* - \bar{w}_{t+1:N}) \\ &\quad + \lambda^{t+1}(\bar{w}_{t+1:N})) + O(\|\bar{\mathbf{w}} - \mathbf{w}^*\|^2) \\ &= [\bar{L}_x^t]^\top + \nabla_{w_t} \lambda^t(\bar{w}_{t:N})(w_t^* - \bar{w}_t) \\ &\quad + [\bar{f}_x^t]^\top \lambda^{t+1}(w_{t+1:N}^*) + O(\|\bar{\mathbf{w}} - \mathbf{w}^*\|^2) \\ &\stackrel{(32),(33)}{=} [\bar{L}_x^t]^\top + (\bar{L}_{xu}^t + \bar{\lambda}_{t+1} \cdot \bar{f}_{xu}^t) (u_t^* - \bar{u}_t) \\ &\quad + (\bar{L}_{xx}^t + \bar{\lambda}_{t+1} \cdot \bar{f}_{xx}^t) (x_t^* - \bar{x}_t) \\ &\quad + [\bar{f}_x^t]^\top (\bar{V}_x^{t+1} + \bar{V}_{xx}^{t+1}) (x_{t+1}^* - \bar{x}_{t+1}) \\ &\quad + [\bar{c}_x^t]^\top (\phi_t^* - \bar{\phi}_t) + O(\|\bar{\mathbf{w}} - \mathbf{w}^*\|^2). \end{aligned} \quad (38)$$

Substituting the expression for x_{t+1}^* in (34) and using identities derived from the backward pass in Sec. V-C yields

$$\begin{aligned} \lambda^t(w_{t:N}^*) &\stackrel{(34),(18)}{=} (\bar{L}_x^t + [V_x^{t+1}]^\top \bar{f}_x^t)^\top + B_t^\top (u_t^* - \bar{u}_t) \\ &\quad + C_t (x_t^* - \bar{x}_t) + [\bar{c}_x^t]^\top (\phi_t^* - \bar{\phi}_t) \\ &\quad + O(\|\bar{\mathbf{w}} - \mathbf{w}^*\|^2). \\ &\stackrel{(19)}{=} (\bar{L}_x^t + [\bar{V}_x^{t+1}]^\top \bar{f}_x^t)^\top + C_t (x_t^* - \bar{x}_t) \\ &\quad - (\beta_t^\top \hat{H}_t + \omega_t^\top A_t^\top) (u_t^* - \bar{u}_t) \\ &\quad - \beta_t^\top A_t (\phi_t^* - \bar{\phi}_t) + O(\|\bar{\mathbf{w}} - \mathbf{w}^*\|^2). \end{aligned} \quad (39)$$

By Theorem 1, $\nabla_{u_t} \mathcal{L}(\mathbf{w}^*, \lambda^*) = 0$, where $\lambda_t^* := \lambda^t(w_{t:N}^*)$. Applying Taylor's theorem, noting that λ^* is a function of \mathbf{w}^* ,

$$\begin{aligned} 0 &= \nabla_{u_t} \mathcal{L}(\mathbf{w}^*, \lambda^*(\mathbf{w}^*)) \\ &\stackrel{(3b)}{=} O(\|\bar{\mathbf{w}} - \mathbf{w}^*\|^2) + [\bar{L}_u^t]^\top - z_t^* + [\bar{f}_u^t]^\top \bar{\lambda}_{t+1} \\ &\quad + (\bar{L}_{uu}^t + \bar{\lambda}_{t+1} \cdot \bar{f}_{uu}^t) (u_t^* - \bar{u}_t) + A_t (\phi_t^* - \bar{\phi}_t) \\ &\quad + (\bar{L}_{ux}^t + \bar{\lambda}_{t+1} \cdot \bar{f}_{ux}^t) (x_t^* - \bar{x}_t) + [\bar{f}_u^t]^\top (\\ &\quad \nabla_{w_{t+1:N}} \lambda^{t+1}(\bar{w}_{t+1:N})(w_{t+1:N}^* - \bar{w}_{t+1:N})) \\ &\stackrel{(37),(33)}{=} O(\|\bar{\mathbf{w}} - \mathbf{w}^*\|^2) + [\bar{L}_u^t]^\top - \mu \bar{U}_t^{-1} e \\ &\quad + (\bar{L}_{uu}^t + \bar{\lambda}_{t+1} \cdot \bar{f}_{uu}^t + \Sigma_t) (u_t^* - \bar{u}_t) \\ &\quad + (\bar{L}_{ux}^t + \bar{\lambda}_{t+1} \cdot \bar{f}_{ux}^t) (x_t^* - \bar{x}_t) + A_t (\phi_t^* - \bar{\phi}_t) \\ &\quad + [\bar{f}_u^t]^\top (\bar{V}_x^{t+1} + \bar{V}_{xx}^{t+1}) (x_{t+1}^* - \bar{x}_{t+1}) \\ &\stackrel{(20),(34),(18)}{=} \hat{Q}_u^t + \hat{H}_t (u_t^* - \bar{u}_t) + B_t (x_t^* - \bar{x}_t) \\ &\quad + A_t (\phi_t^* - \bar{\phi}_t) + O(\|\bar{\mathbf{w}} - \mathbf{w}^*\|^2). \end{aligned} \quad (40)$$

Using (40) and (23a), we can derive an expression for $(\bar{L}_x^t + [\bar{V}_x^{t+1}]^\top \bar{f}_x^t)^\top$. Substituting into (39) yields

$$\begin{aligned} \lambda^t(w_{t:N}^*) &\stackrel{(40),(23a)}{=} \bar{V}_x^t + (C_t + \beta_t^\top B_t)(x_t^* - \bar{x}_t) - \omega_t^\top \bar{c}^t \\ &\quad - \omega_t^\top A_t^\top (u_t^* - \bar{u}_t) + O(\|\bar{\mathbf{w}} - \mathbf{w}^*\|^2) \\ &\stackrel{(35)}{=} \bar{V}_x^t + (C_t + \beta_t^\top B_t + \omega_t^\top \bar{c}_x^t)(x_t^* - \bar{x}_t) \\ &\quad + O(\|\bar{\mathbf{w}} - \mathbf{w}^*\|^2) \\ &\stackrel{(23)}{=} \bar{V}_x^t + \bar{V}_{xx}^t(x_t^* - \bar{x}_t) + O(\|\bar{\mathbf{w}} - \mathbf{w}^*\|^2), \end{aligned} \quad (41)$$

as required. \blacksquare

Corollary 1. *Under Assumptions 1,*

$$\begin{aligned} \hat{Q}_u^t &= -\hat{H}(u_t^* - \bar{u}_t) - B_t(x_t^* - \bar{x}_t) \\ &\quad - A_t(\phi_t^* - \bar{\phi}_t) + O(\|\bar{\mathbf{w}} - \mathbf{w}^*\|^2). \end{aligned} \quad (42)$$

Proof: The result follows immediately from (40). \blacksquare

We now present our main result, which shows that when the current iterate is sufficiently close to a perturbed KKT point, the simplified IPDDP2 algorithm converges to the perturbed KKT point at a quadratic rate.

Theorem 2. *Under Assumptions 1, there exists some $\epsilon > 0$ and $M \geq 0$ such that if $\|\bar{\mathbf{w}} - \mathbf{w}^*\| < \epsilon$,*

$$\|\mathbf{w}^+ - \mathbf{w}^*\| \leq M\|\bar{\mathbf{w}} - \mathbf{w}^*\|^2, \quad (43)$$

and furthermore,

$$\|\mathbf{w}^+ - \mathbf{w}^*\| \leq \|\bar{\mathbf{w}} - \mathbf{w}^*\|. \quad (44)$$

Proof: For any $t \in [N]$ let $S_t := -A_t^\top \hat{H}_t^{-1} A_t$. Assumption (1B) and ((1C)) ensures \hat{H}_t exists and S_t is non-singular. Rearranging the block linear system (19) for ψ_t and ω_t yields

$$\begin{aligned} \psi_t &\stackrel{(19)}{=} S_t^{-1} \left(-\bar{c}^t + A_t^\top \hat{H}_t^{-1} \hat{g}_t \right) \\ &\stackrel{(35),(42)}{=} S_t^{-1} \left(A_t^\top (u_t^* - \bar{u}_t) + \bar{c}_x^t (x_t^* - \bar{x}_t) - A_t^\top \hat{H}_t^{-1} \left(\hat{H}_t (u_t^* - \bar{u}_t) + B_t (x_t^* - \bar{x}_t) + A_t (\phi_t^* - \bar{\phi}_t) \right) \right. \\ &\quad \left. + O(\|\bar{\mathbf{w}} - \mathbf{w}^*\|^2) \right) \\ &= \phi_t^* - \bar{\phi}_t + S_t^{-1} \left(\bar{c}_x^t - A_t^\top \hat{H}_t^{-1} B_t \right) (x_t^* - \bar{x}_t) \\ &\quad + O(\|\bar{\mathbf{w}} - \mathbf{w}^*\|^2) \end{aligned} \quad (45)$$

and $\omega_t = S_t^{-1} \left(-\bar{c}_x^t + A_t^\top \hat{H}_t^{-1} B_t \right)$. Applying the forward pass, with $\gamma = 1$, it follows that

$$\begin{aligned} \phi_t^+ &\stackrel{(24)}{=} \bar{\phi}_t + \psi_t + \omega_t (x_t^+ - \bar{x}_t) \\ &\stackrel{(45)}{=} \bar{\phi}_t + S_t^{-1} \left(\bar{c}_x^t - A_t^\top \hat{H}_t^{-1} B_t \right) (x_t^+ - \bar{x}_t) \\ &\stackrel{(1B)}{=} \phi_t^* + O(\max(\|x_t^+ - x_t^*\|, \|\bar{\mathbf{w}} - \mathbf{w}^*\|^2)), \end{aligned} \quad (46)$$

where the third line follows since S_t^{-1} is bounded by Assumption (1B) and (1C). Similarly, rearranging (19) for α_t and β_t yields

$$\begin{aligned} \alpha_t &\stackrel{(19)}{=} \hat{H}_t^{-1} \left(-\hat{Q}_u^t - A_t \psi_t \right) \\ &\stackrel{(42),(45)}{=} u_t^* - \bar{u}_t + \hat{H}_t^{-1} B_t (x_t^* - \bar{x}_t) \\ &\quad - \hat{H}_t^{-1} A_t (\bar{\phi}_t + \psi_t - \phi_t^*) + O(\|\bar{\mathbf{w}} - \mathbf{w}^*\|^2) \end{aligned} \quad (47)$$

and $\beta_t \stackrel{(19)}{=} \hat{H}_t^{-1} (-B_t - A_t \omega_t)$. Applying the forward pass,

$$\begin{aligned} u_t^+ &\stackrel{(24)}{=} \bar{u}_t + \alpha_t + \beta_t (x_t^+ - \bar{x}_t) \\ &\stackrel{(47)}{=} u_t^* + \hat{H}_t^{-1} B_t (x_t^+ - x_t^*) - \hat{H}_t^{-1} A_t (\phi_t^+ - \phi_t^*) \\ &\quad + O(\|\bar{\mathbf{w}} - \mathbf{w}^*\|^2) \\ &\stackrel{(46),(1B)}{=} u_t^* + O(\max(\|x_t^+ - x_t^*\|, \|\bar{\mathbf{w}} - \mathbf{w}^*\|^2)). \end{aligned} \quad (48)$$

Finally, the forward pass for z_t^+ yields

$$\begin{aligned} z_t^+ &\stackrel{(24)}{=} \bar{z}_t + \chi_t + \zeta_t (x_t^+ - \bar{x}_t) \\ &\stackrel{(21)}{=} \mu \bar{U}_t^{-1} e - \Sigma_t (\alpha_t + \beta_t (x_t^+ - \bar{x}_t)) \\ &\stackrel{(37)}{=} z_t^* + \Sigma_t (u_t^* - u_t^+) + O(\|\bar{\mathbf{w}} - \mathbf{w}^*\|^2) \\ &\stackrel{(48)}{=} z_t^* + O(\max(\|x_t^+ - x_t^*\|, \|\bar{\mathbf{w}} - \mathbf{w}^*\|^2)). \end{aligned} \quad (49)$$

It remains to show that $x_t^+ - x_t^* = O(\|\bar{\mathbf{w}} - \mathbf{w}^*\|^2)$ for all $t \in [N]$, which we do using an inductive argument. The base case of $t = 1$ holds since $x_1^+ = x_1^* = \hat{x}_1$. Now suppose $x_t^+ - x_t^* = O(\|\bar{\mathbf{w}} - \mathbf{w}^*\|^2)$ for some $t \in [N - 1]$. Then by (46), (48) and (49), it follows that $w_t^+ - w_t^* = O(\|\bar{\mathbf{w}} - \mathbf{w}^*\|^2)$ and $w_t^+ - \bar{w}_t = w_t^* - \bar{w}_t + O(\|\bar{\mathbf{w}} - \mathbf{w}^*\|^2)$.

Taylor's theorem yields

$$x_{t+1}^+ = \bar{x}_{t+1} + \bar{f}_x^t (x_t^+ - \bar{x}_t) + \bar{f}_u^t (u_t^+ - \bar{u}_t) + O(\|w_t^+ - \bar{w}_t\|^2), \quad (50)$$

from which we can subtract (50) to yield $x_{t+1}^+ - x_{t+1}^* = O(\|\bar{\mathbf{w}} - \mathbf{w}^*\|^2)$. As a result, $x_t^+ - x_t^* = O(\|\bar{\mathbf{w}} - \mathbf{w}^*\|^2)$ for all $t \in [N]$. It follows immediately that $w_t^+ - w_t^* = O(\|\bar{\mathbf{w}} - \mathbf{w}^*\|^2)$ for all $t \in [N]$, which is equivalent to $\mathbf{w}^+ - \mathbf{w}^* = O(\|\bar{\mathbf{w}} - \mathbf{w}^*\|^2)$. By setting M as the constant in the residual term, we have shown (43) holds.

Finally, to show (44), we select $\epsilon < 1/M$ and substitute $\|\bar{\mathbf{w}} - \mathbf{w}^*\| < \epsilon$ into (43) for the desired result. \blacksquare

VII. NUMERICAL SIMULATIONS

We evaluate IPDDP2 on five motion planning tasks, which involve optimal control problems (OCP) with nonlinear constraints: 1) a minimum work double integrator, 2) a soft-constrained car obstacle avoidance problem, 3) a contact-implicit cartpole swing-up task with Coulomb friction, 4) a contact-implicit acrobot swing-up problem with joint limits and 5) a contact-implicit non-prehensile manipulation task.

A. Comparison Methods

IPDDP2 is compared against IPOPT version 3.14.16 [44] with the MUMPS linear solver version 5.7.3, as well as the recent, state-of-the-art constrained DDP algorithm Prox-DDP [42]. For ProxDDP and IPDDP2, the state trajectories \mathbf{x} are not independent decision variables, whereas they are for IPOPT. For IPDDP2, we use the Julia Symbolics.jl package to compute function derivatives. For ProxDDP and IPOPT, we compute function derivatives using CasADi [60] and reverse-mode automatic differentiation from the JuMP.jl package [61], respectively. IPDDP2 uses full second-order derivatives of all functions, whereas ProxDDP ignores second-order derivatives of the dynamics and constraints. For IPOPT, we include results two variations, one using full second-order derivatives and one using an L-BFGS Hessian approximation [53, Ch. 6.1].

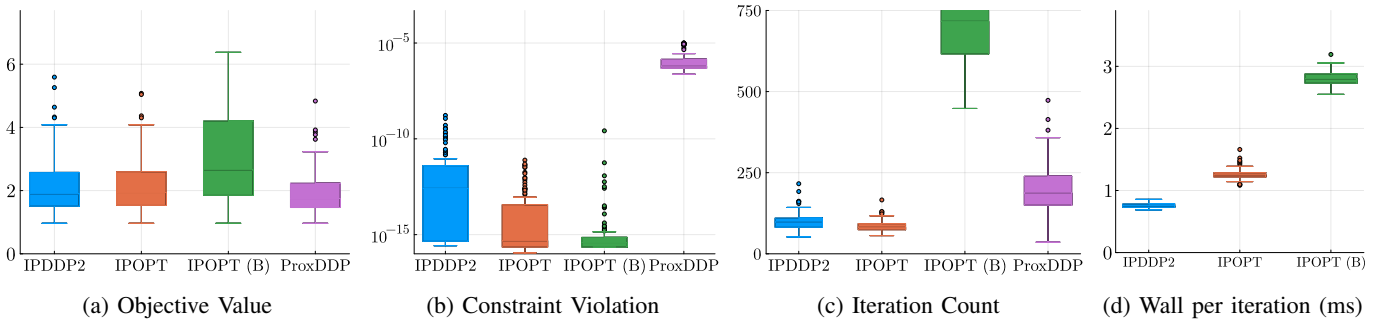


Fig. 1: Summary results for the car obstacle avoidance task (quadratic penalty).

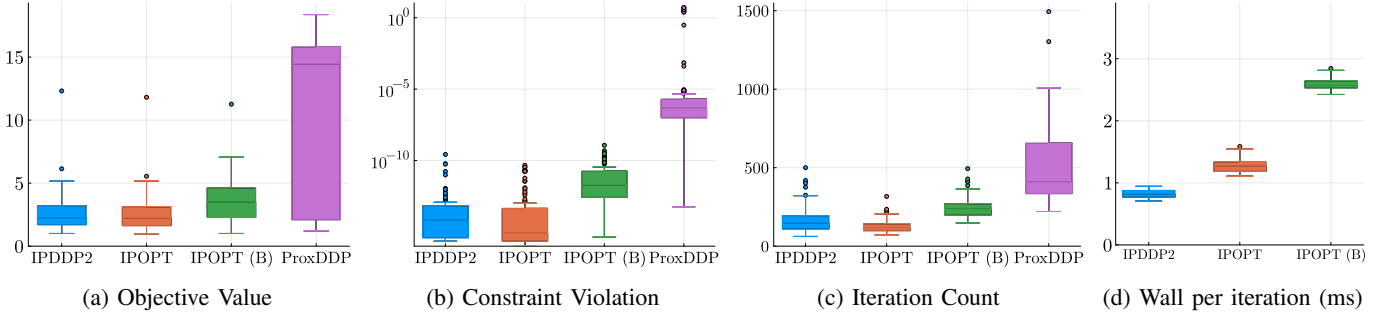


Fig. 2: Summary results for the car obstacle avoidance task (linear penalty) .

In our experiments, we report both wall clock time (total computation time) and solver time (total computation time excluding function and derivative evaluations) for IPDDP2 and IPOPT. For ProxDDP, we do not report timing results since we used the (slower) Python interface. We note that ProxDDP will likely be faster per iteration compared to IPDDP2 since it only requires first-order derivatives.

B. Experimental Setup

The parameter values used for IPDDP2 are $\mu_{\text{init}} = 1.0$, $\kappa_\epsilon = 10.0$, $\kappa_\mu = 0.2$, $\theta_\mu = 1.2$, $\eta_{\mathcal{L}} i = 10^{-4}$, $s_{\mathcal{L}} = 2.3$, $s_\theta = 1.1$, $\delta = 1.0$, $\tau_{\text{min}} = 0.99$, $\gamma_\theta = 10^{-5}$, and $\gamma_{\mathcal{L}} = 10^{-5}$. We set $\theta_{\text{min}} = 10^{-4}\theta(\mathbf{w}_0)$ and $\theta_{\text{max}} = 10^4\theta(\mathbf{w}_0)$ and $\gamma^{\text{min}} = 2 \times 10^{-16}$. Dual variables are initialised with $z_{0,1:N} = e$ and $\phi_{0,1:N} = 0e$. Parameters for the backward pass inertia correction follow the default values from [44].

All methods are provided with the same initial state and control trajectories across all OCPs. IPOPT and IPDDP2 are limited to 1,000 iterations and ProxDDP is limited to 3,000 iterations. We set an optimality error tolerance of 10^{-7} for IPDDP2 and IPOPT and 10^{-5} for first-order methods ProxDDP and IPOPT w/L-BFGS. We tuned the initial AL parameter μ_0 of ProxDDP per motion planning problem to minimise iteration count if feasible solutions are found. Otherwise, constraint violation is minimised. The default parameters for IPDDP2 and IPOPT were used for all problems.

For each of the motion planning problems (excluding double integrator), we create 100 OCPs by varying the dynamics parameters (e.g., pendulum lengths and masses for acrobot) and actuation limits. For all OCPs, $N = 101$ and time discretisation

$\Delta = 0.05$, except for the pushing task, where $\Delta = 0.04$, following Moura et al. [17]. All experiments were limited to one CPU core and performed on a computer with a 4.7GHz AMD Ryzen 9 7900X 12-core processor, Ubuntu 22.04.2 LTS and Julia version 1.11.2.

C. Minimum Work Double Integrator

a) *Problem Description:* This toy problem involves pushing a point mass one unit of distance along a frictionless surface, starting and finishing at rest. The control is a force directly applied to the point mass. The objective function penalises the total absolute work and the analytical solution is known to be a bang-bang policy (see [1]).

Let $x_t = [p_t, v_t]^\top \in \mathbb{R}^2$, $\hat{x}_1 = [0, 0]$ and $u_t = [F_t, s_t^+, s_t^-]^\top \in \mathbb{R}^3$, where $-10 \leq F_t \leq 10$ represents the pushing force and $s_t^+, s_t^- \geq 0$ are slack variables representing the magnitude of the positive and negative components of work at time step t . We enforce the nonlinear constraint $s_t^+ - s_t^- - F_t v_t = 0$ along with $s_t^+, s_t^- \geq 0$. We set $f(x_t, u_t) = [p_t + \Delta v_t, v_t + \Delta F_t]^\top$, $\ell^t(x_t, u_t) = \Delta(s_t^+ + s_t^-)$ for $t < N$ and $\ell^N(x_N, u_N) = 500\|x_N - \hat{x}_N\|_2^2$, where $\hat{x}_N = [1, 0]^\top$. Variables are initialised with $F_t, s_t^+, s_t^- = 0.01$.

Despite the problem seeming overly simplistic, we show in the following that it causes a great deal of difficulty for first-order methods such as ProxDDP and IPOPT w/L-BFGS.

b) *Results:* All methods recover the analytical bang-bang policy. ProxDDP and IPOPT (B) are first-order methods, and as such require significantly more iterations compared to IPDDP2 and IPOPT to converge to a solution.

TABLE I: Results for Double Integrator

	Iterations	$J(\mathbf{x}^*, \mathbf{u}^*)$	$\theta(\mathbf{w}^*)$	Wall (ms)	Solver (ms)
ProxDDP	294	1.266	2.9×10^{-6}	-	-
IPOPT (B)	143	1.266	3.7×10^{-9}	902.8	882.6
IPOPT	28	1.266	3.1×10^{-8}	9.6	9.6
IPDDP2	31	1.266	3.0×10^{-10}	11.9	7.9

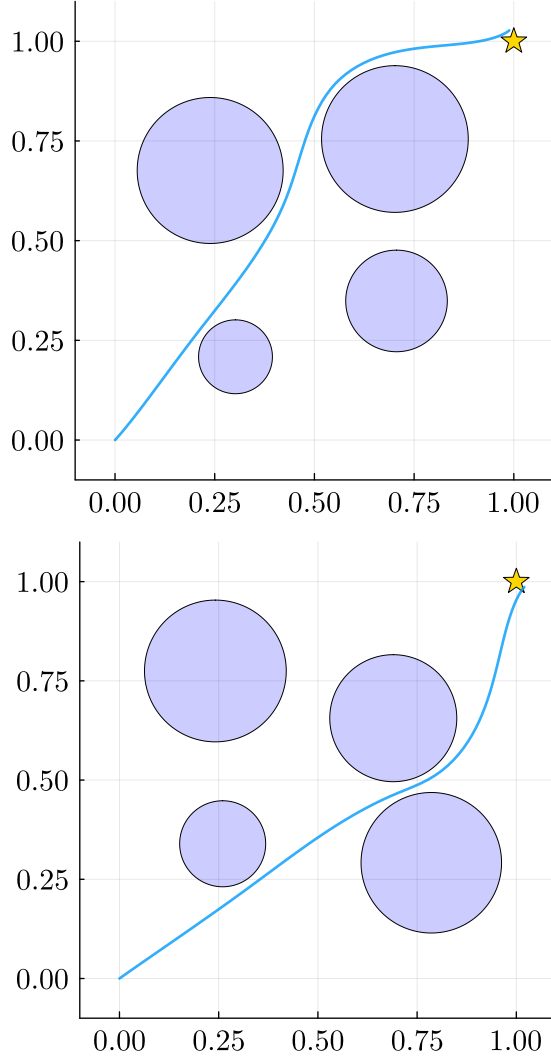


Fig. 3: Illustration of two different OCPs solved for the car obstacle avoidance problem. The star marks the goal location.

D. Car Obstacle Avoidance

a) *Problem Description*: Our first problem involves navigating a car to a goal pose while avoiding four obstacles. Let $x_t = [p_t^x, p_t^y, \theta_t, v_t]^\top \in \mathbb{R}^4$ include the 2D car pose and forward velocity at time step t , and let $u_t = [F_t, \tau_t, s_t^1, s_t^2, s_t^3, s_t^4]^\top \in \mathbb{R}^6$ include the forward acceleration force F_t and steering torque τ_t as well as slack variables for the obstacle constraints, denoted by $s_t = [s_t^1, s_t^2, s_t^3, s_t^4]^\top$, respectively, at time step t . The car dynamics obey the nonlinear vehicle model, described by $\dot{x} = g(x, u) := [v \cos \theta, v \sin \theta, \tau, F]^\top$. We convert the continuous time equa-

tion to a discrete-time dynamics equation using the (second-order) explicit midpoint method, i.e., $x_{t+1} = f(x_t, u_t) := x_t + \Delta g(x_t + \frac{\Delta}{2} g(x_t, u_t), u_t)$.

The circular obstacles are represented by their centre position and radius, i.e., (o_i^x, o_i^y, o_i^r) for $i \in [4]$, with positions of each obstacle uniformly sampled across each of the four quadrants in $[0, 1]^2$ and its radius uniformly sampled between $[0, 0.5, 0.2]$. The car also has radius $r_{\text{car}} = 0.02$. The obstacle constraints are given by $s_t^i \geq 0$ and

$$(p_t^x - o_i^x)^2 + (p_t^y - o_i^y)^2 - (o_i^r + r_{\text{car}})^2 \leq s_t^i \quad (51)$$

for all i, t . We also include control limits selected at random for each OCP according to $u_t \in [-F^{\text{lim}}, F^{\text{lim}}] \times [-\tau^{\text{lim}}, \tau^{\text{lim}}]$, where $F^{\text{lim}} \sim \mathcal{U}(1.5, 2.5)$ and $\tau^{\text{lim}} \sim \mathcal{U}(3, 5)$.

For the objective function, we set

$$\begin{aligned} \ell^t(x_t, u_t) &= 0.1\Delta(5F_t^2 + \tau_t^2) + p(s_t), \quad t < N \\ \ell^N(x_N, u_N) &= 200\|x_N - \hat{x}_N\|^2, \quad \hat{x}_N = [1, 1, \pi/4, 0]^\top, \end{aligned} \quad (52)$$

where p is a penalty function on the slacks. We present results for two variants for p : a linear penalty, i.e., $p(s_t) = 50s_t^\top e$ and a quadratic penalty, i.e., $p(s_t) = 10^3\|s_t\|_2^2$.

The initial state is given by $\hat{x}_1 = [0, 0, \theta_1, 0]^\top$, where $\theta_1 \sim \mathcal{U}(\pi/8, 3\pi/8)$. We initialise controls with $F_t, \tau_t = 0$ and slacks variables $s_t = 0.01$ for all t . This obstacle avoidance problem follows a *soft-constraint* formulation which arises in the MPC literature, e.g., [23, Ch. 1.2] and [62], where constraint violation is allowed (but penalised) through the slack variables s_t . We set the objective weight for the linear slack variables high enough such that no constraint violation is observed in practice. This is possible since the linear penalty is an *exact penalty* [62].

b) *Results (Quadratic Penalty)*: IPDDP2 and IPOPT find similar solutions across all 100 OCPs, with slightly lower variation in solution quality for IPDDP2. IPOPT w/L-BFGS finds slightly higher cost solutions compared to other methods, and yields occasional constraint violation. ProxDDP is able to find on average, lower cost solutions compared to other methods at the expense of a small degree of constraint violation. Both first-order methods (IPOPT w/L-BFGS and ProxDDP) require a higher iteration count compared to IPDDP2 and IPOPT. While IPDDP2 requires on average 13% more iterations compared to IPOPT, the overall wall clock per iteration is on average 60% of IPOPT. Furthermore, wall clock per iteration of IPDDP2 is only 27% of IPOPT w/L-BFGS. Fig. 1 presents the summary of the results for this task.

c) *Results (Linear Penalty)*: For the more challenging linear penalty case, IPDDP2 and IPOPT are able to find locally optimal solutions to all 100 OCPs. Similar to the quadratic penalty case, IPOPT w/L-BFGS finds slightly higher cost solutions. ProxDDP however, finds significantly higher cost solutions overall and requires a significantly higher iteration count compared to other methods. Furthermore, ProxDDP failed to find feasible solutions for 10 out of the 100 OCPs. While IPDDP2 requires on average 17% more iterations compared to IPOPT, the overall wall clock per iteration is on average 64% of IPOPT. Furthermore, wall clock per iteration of IPDDP2 is

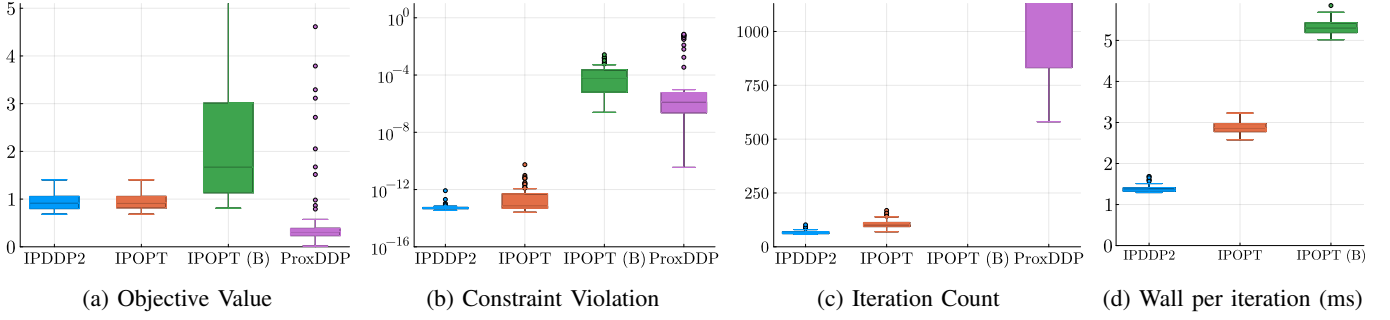


Fig. 4: Summary results for the cartpole swing-up task with Coulomb friction.

only 32% of IPOPT w/L-BFGS. Fig. 2 presents the summary of the results for this task and we provide some qualitative examples in Fig. 3.

E. Cartpole Swing-Up with Coulomb Friction

a) *Problem Description:* This task is the cartpole swing-up task with Coulomb friction applying to both the cart and the pendulum, introduced by [37]. Frictional forces are derived using the principle of maximum dissipation, which is adapted to discrete-time optimal control problems through a variational time-stepping framework [35, 38]. Under this framework, frictional forces are resolved jointly with the rigid-body dynamics for each discrete time step by introducing (nonlinear) constraints.

Let $q_t = [p_t, \theta_t]^\top \in \mathbb{R}^2$ represent the configuration of the cartpole at time step t and let $q_t^-, q_t^+ \in \mathbb{R}^2$ be the configurations at the prior and subsequent time steps. Let states $x_t = (q_t^-, q_t) \in \mathbb{R}^4$, $\hat{x}_1 = [0, 0, 0, 0]^\top$ and $u_t = (F_t, q_t^+, \beta_t^c, \beta_t^p, \psi_t, s_t, s_t^c, s_t^p) \in \mathbb{R}^{15}$, where $F_t \in [-10, 10]$ is the cart actuation force, $\beta_t^c, \beta_t^p \in \mathbb{R}^2$ represent (overparameterised) frictional forces, $\psi_t \in \mathbb{R}^2$ are dual variables associated with friction and finally, $s_t, s_t^c, s_t^p \in \mathbb{R}^2$ are slack variables associated with the complementarity constraints. The discrete time dynamics are given by $x_{t+1} = f(x, u) := (q_t, q_t^+)$.

Following [35, 37], we set the following constraints for each time step:

$$\widehat{M}(q_t^-, q_t, q_t^+) + \widehat{C}(q_t^-, q_t, q_t^+) = BF_t + J_C^\top \lambda_t, \quad (53a)$$

$$\psi_t \odot (c_f \gamma - [\beta_t^c \ \beta_t^p]^\top e) - s_t = 0, \quad (53b)$$

$$\beta_t^c \odot (Pq_t^{vm+} + \psi_t^{(1)} e) - s_t^c = 0, \quad (53c)$$

$$\beta_t^p \odot (Pq_t^{vm+} + \psi_t^{(2)} e) - s_t^p = 0, \quad (53d)$$

$$\beta_t^c, \beta_t^p, Pq_t^{vm+} + \psi_t^{(1)} e, Pq_t^{vm+} + \psi_t^{(2)} e \geq 0, \quad (53e)$$

$$\psi_t, c_f \gamma - [\beta_t^c \ \beta_t^p]^\top e, s_t, s_t^c, s_t^p \geq 0. \quad (53f)$$

(53a) are the rigid body dynamics of the cartpole system including frictional forces $\lambda_t \in \mathbb{R}^2$, which are given by $\lambda_t^{(1)} = [\beta_t^c]^{(1)} - [\beta_t^c]^{(2)}$ and $\lambda_t^{(2)} = [\beta_t^p]^{(1)} - [\beta_t^p]^{(2)}$. $c_f := [c_f^c, c_f^p]^\top$ are the coefficients of friction for each contact point and γ are the normal forces for each contact, which are assumed constant

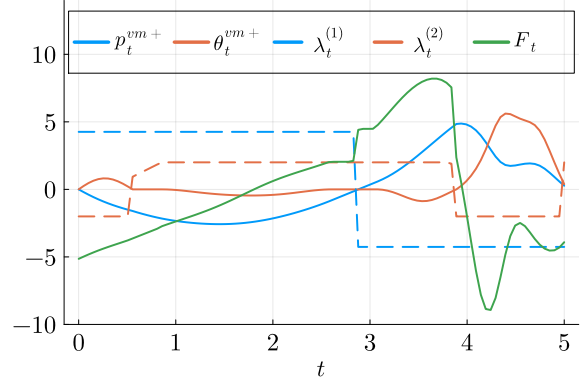


Fig. 5: An example solution for the cartpole problem. p_t^{vm+} and θ_t^{vm+} represent the forward difference approximation of the cart and pole velocities, respectively, and λ_t^c, λ_t^p are the corresponding frictional forces. Note how frictional forces oppose the direction of motion for each contact and have a magnitude based on the limit of the friction cone.

following [37]. Furthermore, \widehat{M}, \widehat{C} are define as

$$\begin{aligned} \widehat{M}(q_t^-, q_t, q_t^+) &:= \frac{M(q_t^{m+})q_t^{vm+} - M(q_t^{m-})q_t^{vm-}}{\Delta}, \\ \widehat{C}(q_t^-, q_t, q_t^+) &:= \frac{C(q_t^{m+}, q_t^{vm+}) + C(q_t^{m-}, q_t^{vm-})}{2}, \end{aligned} \quad (54)$$

and

$$\begin{aligned} q_t^{m-} &:= \frac{q_t^- + q_t}{2}, & q_t^{m+} &:= \frac{q_t + q_t^+}{2}, \\ q_t^{vm-} &:= \frac{q_t - q_t^-}{\Delta}, & q_t^{vm+} &:= \frac{q_t^+ - q_t}{\Delta}. \end{aligned} \quad (55)$$

Finally, B, J_C are the control and contact Jacobian, and $M(q), C(q, \dot{q})$ are the mass matrix and Coriolis terms for the cartpole system. For each of the 100 OCPs derived from the cartpole task, we randomly sample the mass of the cart and pole (m_c, m_p), length of the pole (l) and friction coefficients (c_f^c, c_f^p) according to $m_c \sim \mathcal{U}(0.9, 1.1)$, $m_p \sim \mathcal{U}(0.9, 1.1)$, $l \sim \mathcal{U}(0.45, 0.55)$ and $c_f^c, c_f^p \sim \mathcal{U}(0.05, 0.15)$.

The objective function is given by

$$\begin{aligned} \ell^t(x_t, u_t) &= 0.01\Delta F_t^2 + (s_t + s_t^c + s_t^p)^\top e, \quad t < N \\ \ell^N(x_N, u_N) &= 500\|q_N - \hat{q}_N\|_2^2 + 200\|q_N^{vm-}\|_2^2, \end{aligned}$$

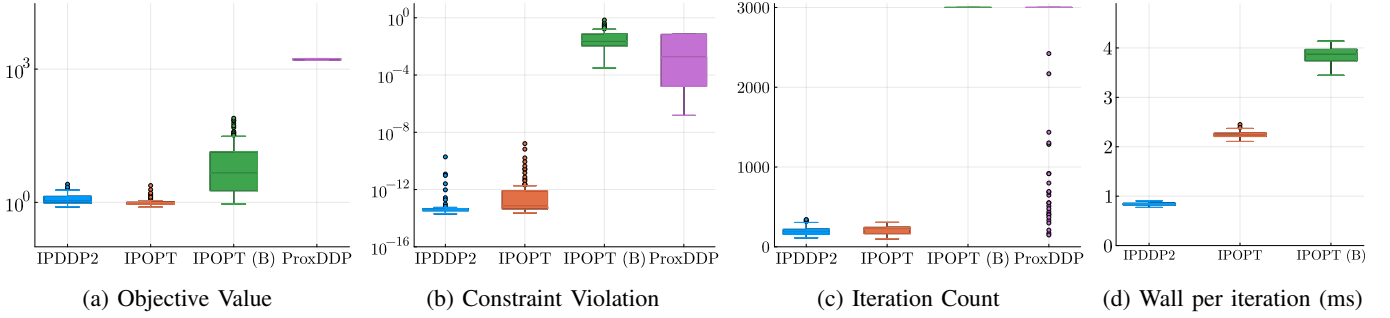


Fig. 6: Summary results for the acrobot swing-up task with joint limits.

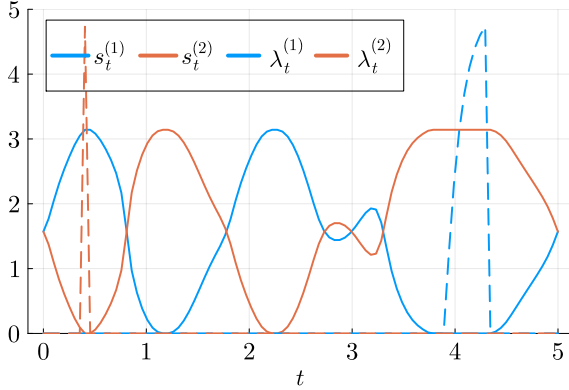


Fig. 7: An example solution for the acrobot problem. s_t is the signed distance to the joint limits and λ_t denotes the impulses. The “switching nature” of the impulses and joint limits are especially notable around the four second mark, where the acrobot is “leaning into” the joint limit.

where $\hat{q}_N = [0, \pi]^\top$. The linear penalty on the slack variables is an exact penalty [35], and in our experiments we observe the final values of the slack variables are always below the solver tolerance. We initialise variables with $F_t, q_t^+ = 0$ and remaining variables equal to 0.01 for all t .

b) Results: IPDDP2 and IPOPT are able to reliably solve the cartpole swing-up task for all 100 OCPs, yielding similar solutions. IPOPT w/L-BFGS yields higher cost solutions overall, as well as some constraint violation when compared to IPDDP2/IPOPT. ProxDDP fails to find a feasible solution for 13 out of 100 of the OCPs. However, for the remaining 87 OCPs, ProxDDP often finds lower cost solutions compared to IPDDP2/IPOPT. We observed significantly higher overall iteration counts and higher variability of iteration counts from ProxDDP compared to IPDDP2/IPOPT. IPDDP2 yields a dramatic speed-up for the cartpole task compared to IPOPT; it requires on average 62% of the iterations compared to IPOPT and in addition, wall clock per iteration is on average 48% of IPOPT. Furthermore, wall clock per iteration of IPDDP2 is 24% of IPOPT w/L-BFGS. Fig. 4 presents the summary of the results for this task and a qualitative example of a solution trajectory in Fig. 5.

F. Acrobot Swing-Up with Joint Limits

a) Problem Description: This task is an acrobot swing-up task, where limits are imposed on the elbow joint, introduced by Howell et al. [37]. The joint limits are enforced by resolving an impulse, which is only applied when a joint limit is reached. Intuitively, the acrobot is allowed to “slam” into either joint limit, and the impulse takes on the appropriate value to ensure the joint limits are not violated. Similar to the cartpole problem, a variational time-stepping framework [35, 37] is applied to encode the contact dynamics.

Let $q_t = [\theta_t^b, \theta_t^e]^\top \in \mathbb{R}^2$ represent the configuration of the acrobot at time step t , i.e., the base and elbow joint angles, and let $q_t^-, q_t^+ \in \mathbb{R}^2$ be the configurations at the prior and subsequent time steps. Let $x_t = (q_t^-, q_t) \in \mathbb{R}^4$, $\hat{x}_1 = [0, 0, 0, 0]^\top$ and $u_t = (\tau_t, q_t^+, \lambda_t, s_t) \in \mathbb{R}^7$, where $\tau_t \in [-10, 10]$ is the elbow torque, $\lambda_t \in \mathbb{R}^2$ represents the impulse at the $+\pi/2$ and $-\pi/2$ joint limits, and finally, $s_t \in \mathbb{R}^2$ are slack variables for time step t .

We apply the (nonlinear) rigid body dynamics constraints

$$\widehat{M}(q_t^-, q_t, q_t^+) + \widehat{C}(q_t^-, q_t, q_t^+) = B\tau_t + J_C^\top \lambda_t - \frac{q_t^{vm+}}{2}, \quad (56)$$

where B and J_C are the control and contact Jacobians which map control and contact forces, respectively, into the configuration space and $q_t^{vm+}/2$ is an additional damping term.

Denoting the signed distance function to joint limits by $\phi(q_t) = [\pi/2 - \theta_t^e, \theta_t^e - \pi/2]^\top$, we apply additional constraints

$$\phi(q_t^+), \lambda_t, s_t \geq 0, \quad \lambda_t \odot \phi(q_t^+) - s_t = 0, \quad (57)$$

in addition to (56). The complementarity constraints in (57) enforce the discontinuous “switching” nature of the impulse and joint limit constraints.

Finally, the objective function is given by

$$\begin{aligned} \ell^t(x_t, u_t) &= 0.01\Delta\tau_t^2 + 2s_t^\top e, \quad t < N \\ \ell^N(x_N, u_N) &= 500\|q_N - \hat{q}_N\|_2^2 + 200\|q_N^{vm-}\|_2^2, \end{aligned} \quad (58)$$

where $\hat{q}_N = [\pi, 0]^\top$. We initialise variables with $\tau_t, q_t^+ = 0$ and $\lambda_t, s_t = 0.01$ for all t .

b) Results: IPOPT and IPDDP2 are able to find locally optimal solutions for all 100 OCPs, with IPOPT yielding lower cost solutions overall. However, IPOPT w/L-BFGS is consistently unable to find feasible solutions. ProxDDP

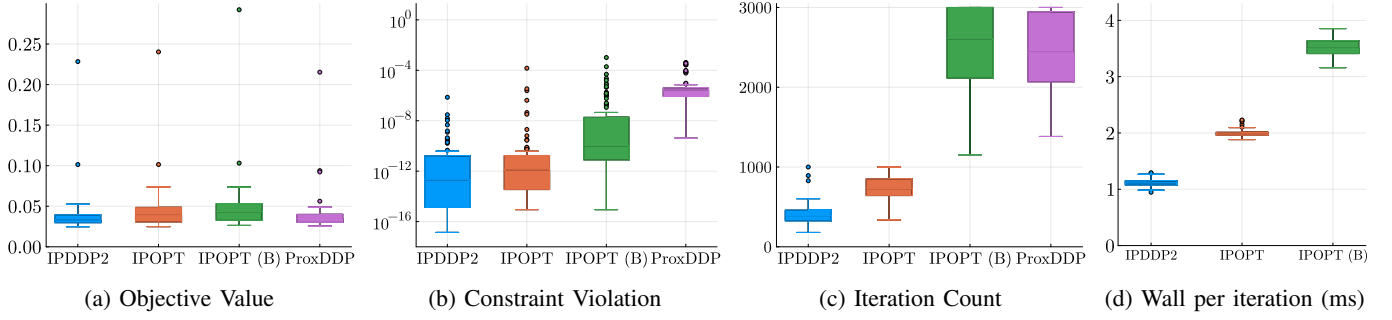


Fig. 8: Summary results for the non-prehensile manipulation task.

consistently finds feasible but significantly higher cost solutions. IPDDP2 requires 6% less iterations compared to IPOPT on average, with wall clock per iteration being on average 37% of IPOPT. Furthermore, the wall clock per iteration of IPDDP2 is 22% of IPOPT w/L-BFGS. Fig. 6 presents the summary of the results for this task and a qualitative example of a solution trajectory in Fig. 7.

G. Non-Prehensile Manipulation

Our final task is a non-prehensile manipulation planning task, described in [17], where a manipulator (the pusher) is tasked with using its end-effector to push a rectangular block (the slider) from a start to a goal configuration, while avoiding an obstacle. The dynamics of the pusher-slider problem includes multiple sticking and sliding contact modes, which are encoded through complementarity constraints.

The states of the system are given by $x_t = [p_t^x, p_t^y, \theta_t, \phi_t]^\top \in \mathbb{R}^4$, where $[p_t^x, p_t^y, \theta_t]^\top$ is the position of the slider in the global coordinate frame, and ϕ_t encodes the position of the pusher relative to the slider. Controls are given by $u_t = [F_t^n, F_t^T, \dot{\phi}_t^+, \dot{\phi}_t^-, s_t^+, s_t^-, s_t^o]^\top \in \mathbb{R}^6$, where F_t^n, F_t^T are the normal and tangential force applied by the pusher to the slider in the contact frame, $\dot{\phi}_t^+, \dot{\phi}_t^-$ are the positive and negative components of the relative velocity of the pusher to the slider, i.e., $\dot{\phi}_t = \dot{\phi}_t^+ - \dot{\phi}_t^-$ and s_t^+, s_t^-, s_t^o are slack variables.

The continuous time dynamics are given by

$$\dot{x} = g(x, u) := \begin{bmatrix} R(\theta)LJ_C(\phi)^\top & 0 & 0 \\ 0 & 1 & -1 \end{bmatrix} u, \quad (59)$$

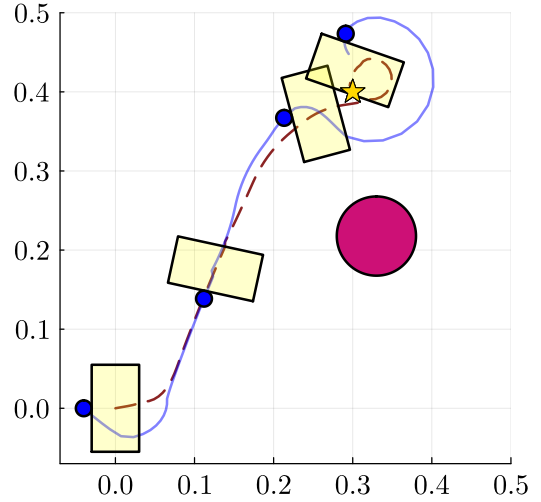
where $L \in \mathbb{R}^{3 \times 3}$ arises from an ellipsoidal approximation of the limit surface of the slide (see [20] for details) and

$$R(\theta) = \begin{bmatrix} \cos(\theta) & -\sin(\theta) & 0 \\ \sin(\theta) & \cos(\theta) & 0 \\ 0 & 0 & 1 \end{bmatrix}, \quad (60)$$

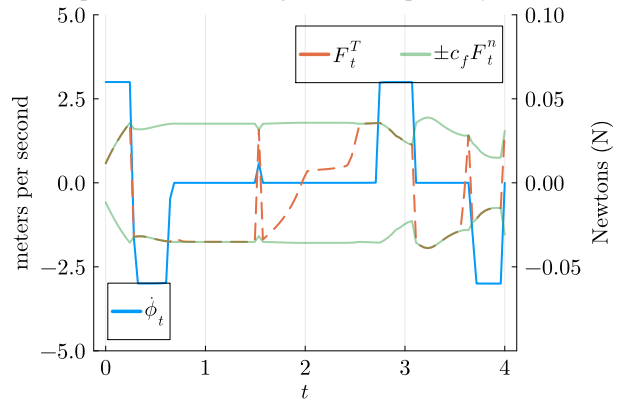
$$J_C = \begin{bmatrix} 1 & 0 & p^x \tan(\phi)/2 \\ 0 & 1 & -p^x/2 \end{bmatrix}.$$

We convert the continuous time equation in (59) to a discrete-time dynamics equation $x_{t+1} = f(x_t, u_t)$ using a forward Euler approximation, following [17].

The forces F_t^n, F_t^T between the pusher and slider, as well as the relative velocities $\dot{\phi}_t$ are subject to constraints imposed by



(a) Visualisation of the pusher and slider trajectories. The pusher and obstacle are the blue and pink circles, respectively, the slider is the yellow block and the star marks the goal location. Blue and brown lines represent the pusher and slider trajectories, respectively.



(b) Visualisation of contact force trajectories. The counter-clockwise velocity between pusher and slider is on the left axes and contact forces are on the right axes. Note how contact modes in (61) are satisfied, i.e., friction forces respect the friction cone and oppose the direction of motion.

Fig. 9: A qualitative example illustrating a single OCP for the non-prehensile manipulation problem.

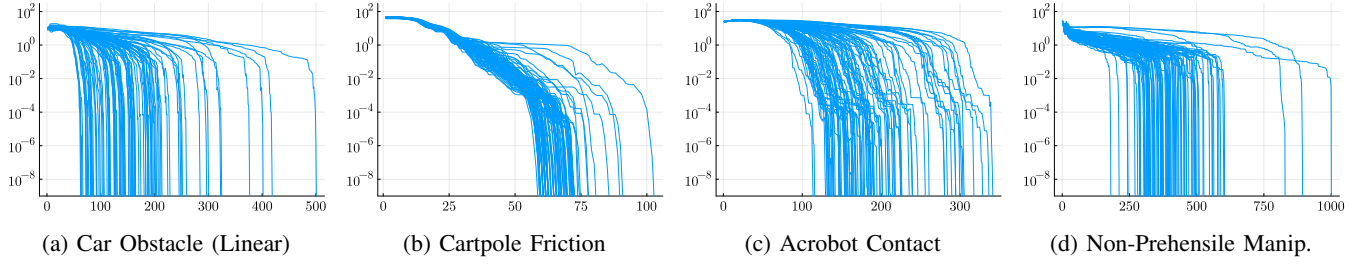


Fig. 10: Empirical validation of the local quadratic convergence of IPDDP2. The x-axis measures iteration count and the y-axis measures $\|u_{k,1:N} - u_{1:N}^*\|_2$, where $u_{1:N}^*$ is the optimal point found by IPDDP2.

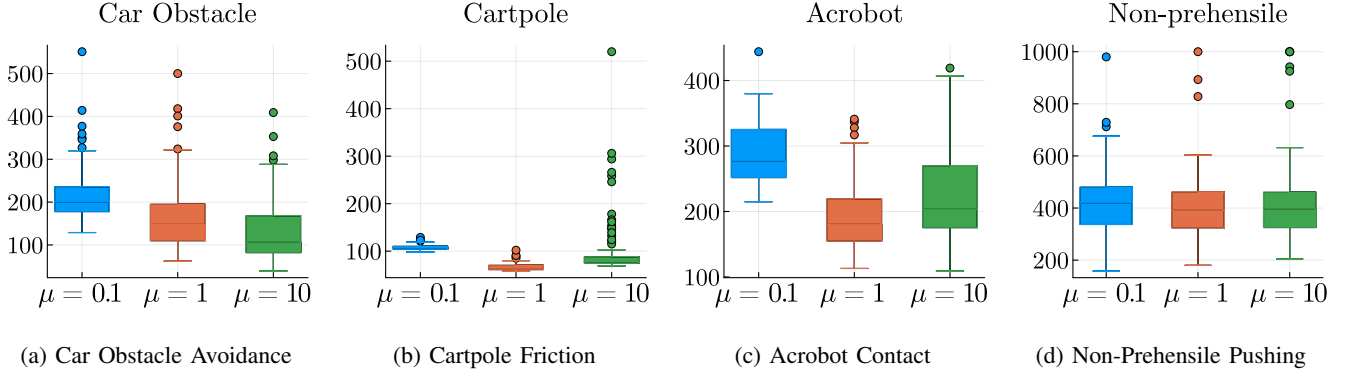


Fig. 11: Ablation of the initial barrier parameter μ_{init} on iteration count. While we observe significant variation in iteration counts, the reliability of convergence is unaffected.

a Coulomb friction model. Specifically, the following contact modes are modeled:

$$\begin{aligned} \dot{\phi}_t = 0 &\implies |F_t^T| \leq c_f F_t^n \quad (\text{sticking contact}) \\ \dot{\phi}_t > 0 &\implies F_t^T = c_f F_t^n \quad (\text{counterclockwise}) \\ \dot{\phi}_t < 0 &\implies F_t^T = -c_f F_t^n \quad (\text{clockwise}), \end{aligned} \quad (61)$$

where counterclockwise (similarly clockwise), stands for a counterclockwise rotation of the pusher relative to the slider. The contact modes in (61) can be encoded through constraints

$$\begin{aligned} (c_f F_t^n - F_t^T) \odot \dot{\phi}_t^- - s_t^- &= 0 \\ (c_f F_t^n + F_t^T) \odot \dot{\phi}_t^+ - s_t^+ &= 0 \\ F_t^n, c_f F_t^n - F_t^T, c_f F_t^n + F_t^T, \dot{\phi}_t^-, \dot{\phi}_t^+, s_t^-, s_t^+ &\geq 0, \end{aligned} \quad (62)$$

where $c_f > 0$ is the coefficient of friction between the pusher and slider. In addition to friction constraints, (soft) obstacle avoidance constraints are included, given by $s_t^o \geq 0$,

$$(p_t^x - o^x)^2 + (p_t^y - o^y)^2 - (o^r + r_{\text{push}})^2 \leq s_t^o, \quad (63)$$

where $r_{\text{push}} = 0.01$ is the radius of the pusher. Finally, we apply the bound constraints $f_t^T \in [-0.3, 0.3]$, $\dot{\phi}_t^+, \dot{\phi}_t^- \in [-3, 3]$ and $\phi_t \in [-0.9, 0.9]$.

The objective function of the pushing task is given by

$$\begin{aligned} \ell^t(x_t, u_t) &= 0.01 ([f_t^n]^2 + [f_t^T]^2) + 2(s_t^+ + s_t^- + s_t^o), \quad t < N \\ \ell^N(x_N, u_N) &= 20\|x_N - \hat{x}_N\|_2^2. \end{aligned} \quad (64)$$

where $\hat{x}_N = [0.3, 0.4, 3\pi/2, 0]^\top$ is the target goal state. The initial state is given by $\hat{x}_1 = [0, 0, 0, 0]^\top$.

For each of the 100 OCPs, the coefficient of friction is sampled according to $c_f \sim \mathcal{U}(0.15, 0.25)$ and the obstacle is initialised randomly and uniformly using $[o_x, o_y] \in [0.05, 0.3] \times [0.15, 0.25]$ and $o_r \sim \mathcal{U}(0.05, 0.07)$. All variables in u_t are initialised to 0.01 for all t .

a) Results: All methods are able to solve all 100 OCPs, with IPDDP2 and ProxDDP finding lower cost solutions overall compared to IPOPT and IPOPT w/L-BFGS. First-order methods ProxDDP and IPOPT w/L-BFGS, require significantly more iterations compared to IPDDP2 and IPOPT. IPDDP2 requires on average 55% of the iterations compared to IPOPT and in addition, the wall clock per iteration is on average 55% of IPOPT. Furthermore, wall clock per iteration of IPDDP2 is 32% of IPOPT w/L-BFGS. Fig. 8 presents the summary of the results for this task and a qualitative example and visualisation of the pushing task in Fig. 9.

H. Discussion

We have shown in this section that IPDDP2 is able to solve OCPs faster than IPOPT, due to its structure-exploiting nature, while offering significant gains in reliability compared to ProxDDP. A further benefit of IPDDP2 compared to IPOPT is that IPDDP2 offers a linear feedback policy which can be used when implementing an NMPC controller. We provide some additional analysis on IPDDP2 to show, 1) that our local quadratic convergence result in Sec. VI is observed in practice and, 2) illustrate the effect of tuning the initial barrier parameter μ_{init} on IPDDP2's performance.

a) *Local Quadratic Convergence*: Fig. 10 plots the convergence of IPDDP2 for all OCPs across four problem classes. Local superlinear convergence is typically observed in practice when sufficiently close to the optimal point $u_{1:N}^*$, validating the formal result in Sec. VI.

b) *Tuning solver parameters*: IPDDP2 has many solver parameters, similar to IPOPT. We observed that the iteration count and solution quality were the most sensitive to the initial barrier parameter μ_{init} and the barrier subproblem convergence tolerance κ_ϵ . In Fig. 11, we show results when the initial barrier parameter is varied from default values.

VIII. CONCLUSION

We conclude the paper with a discussion of promising avenues for future work around IPDDP2.

a) *Feasibility Restoration Phase*: IPOPT [44] includes a *feasibility restoration phase* which is invoked when either, 1) the backtracking line search fails to find an acceptable iterate or, 2) the KKT system is severely ill-conditioned. The purpose of the feasibility restoration phase is to find a point acceptable to the filter by searching for a feasible point (while neglecting the objective function). Developing a similar restoration phase for IPDDP2 would improve the robustness of the implementation.

b) *Integration of Rigid-Body Dynamics Libraries*: In addition to the above, integrating libraries for evaluating rigid body dynamics and their derivatives [63] into the current implementation would enable deployment of IPDDP2 on hardware in NMPC controllers for legged robots and manipulators. We anticipate it will be particularly important to include second-order derivatives when integrating these libraries, which can be achieved in an efficient manner for rigid-body systems [64].

ACKNOWLEDGMENTS

REFERENCES

- [1] M. Kelly, “An Introduction to Trajectory Optimization: How to Do Your Own Direct Collocation,” *SIAM Review*, vol. 59, no. 4, pp. 849–904, 2017.
- [2] J. T. Betts, *Practical Methods for Optimal Control and Estimation Using Nonlinear Programming*. Advances in Design and Control, Society for Industrial and Applied Mathematics, second ed., 2010.
- [3] C. Kellett and P. Braun, *Introduction to Nonlinear Control: Stability, Control Design, and Estimation*. Princeton University Press, 2023.
- [4] J. Rawlings, D. Mayne, and M. Diehl, *Model Predictive Control: Theory, Computation, and Design*. Nob Hill Publishing, 2nd ed., 2020.
- [5] P. Foehn, A. Romero, and D. Scaramuzza, “Time-optimal planning for quadrotor waypoint flight,” *Science Robotics*, vol. 6, no. 56, 2021.
- [6] J. Y. Goh, T. Goel, and J. Christian Gerdes, “Toward Automated Vehicle Control Beyond the Stability Limits: Drifting Along a General Path,” *Journal of Dynamic Systems, Measurement, and Control*, vol. 142, p. 021004, 11 2019.
- [7] P. M. Wensing, M. Posa, Y. Hu, A. Escande, N. Mansard, and A. D. Prete, “Optimization-based control for dynamic legged robots,” *IEEE Transactions on Robotics*, vol. 40, pp. 43–63, 2024.
- [8] F. Farshidian, E. Jelavic, A. Satapathy, M. Gifftthaler, and J. Buchli, “Real-time motion planning of legged robots: A model predictive control approach,” in *IEEE-RAS 17th International Conference on Humanoid Robotics (Humanoids)*, pp. 577–584, 2017.
- [9] R. Grandia, F. Jenelten, S. Yang, F. Farshidian, and M. Hutter, “Perceptive locomotion through nonlinear model-predictive control,” *IEEE Transactions on Robotics*, vol. 39, no. 5, pp. 3402–3421, 2023.
- [10] A. W. Winkler, C. D. Bellicoso, M. Hutter, and J. Buchli, “Gait and trajectory optimization for legged systems through phase-based end-effector parameterization,” *IEEE Robotics and Automation Letters*, vol. 3, no. 3, pp. 1560–1567, 2018.
- [11] C. Mastalli, S. P. Chhatoi, T. Corbères, S. Tonneau, and S. Vijayakumar, “Inverse-Dynamics MPC via Nullspace Resolution,” *IEEE Transactions on Robotics*, vol. 39, no. 4, pp. 3222–3241, 2023.
- [12] J. Zeng, B. Zhang, and K. Sreenath, “Safety-critical model predictive control with discrete-time control barrier function,” in *American Control Conference (ACC)*, pp. 3882–3889, 2021.
- [13] X. Zhang, A. Liniger, A. Sakai, and F. Borrelli, “Autonomous parking using optimization-based collision avoidance,” in *IEEE Conference on Decision and Control (CDC)*, pp. 4327–4332, 2018.
- [14] X. Zhang, A. Liniger, and F. Borrelli, “Optimization-based collision avoidance,” *IEEE Transactions on Control Systems Technology*, vol. 29, no. 3, pp. 972–983, 2021.
- [15] T. Marcucci, M. Petersen, D. von Wrangel, and R. Tedrake, “Motion planning around obstacles with convex optimization,” *Science Robotics*, vol. 8, no. 84, p. eadf7843, 2023.
- [16] T. Xue, H. Girgin, T. S. Lembono, and S. Calinon, “Demonstration-guided optimal control for long-term non-prehensile planar manipulation,” in *IEEE International Conference on Robotics and Automation (ICRA)*, pp. 4999–5005, 2023.
- [17] J. Moura, T. Stouraitis, and S. Vijayakumar, “Non-prehensile planar manipulation via trajectory optimization with complementarity constraints,” in *IEEE International Conference on Robotics and Automation (ICRA)*, pp. 970–976, 2022.
- [18] J.-P. Sleiman, F. Farshidian, M. V. Minniti, and M. Hutter, “A Unified MPC Framework for Whole-Body Dynamic Locomotion and Manipulation,” *IEEE Robotics and Automation Letters*, vol. 6, no. 3, pp. 4688–4695, 2021.
- [19] W. Yang and M. Posa, “Dynamic On-Palm Manipulation via Controlled Sliding,” in *Proceedings of Robotics: Science and Systems*, (Delft, Netherlands), July 2024.
- [20] F. R. Hogan and A. Rodriguez, “Reactive planar non-prehensile manipulation with hybrid model predictive

- control,” *The International Journal of Robotics Research*, vol. 39, no. 7, pp. 755–773, 2020.
- [21] J. J. A. Zanelli, A. Domahidi and M. Morari, “FORCES NLP: an efficient implementation of interior-point methods for multistage nonlinear nonconvex programs,” *International Journal of Control*, vol. 93, no. 1, pp. 13–29, 2020.
- [22] B. Houska, H. Ferreau, and M. Diehl, “ACADO Toolkit – An Open Source Framework for Automatic Control and Dynamic Optimization,” *Optimal Control Applications and Methods*, vol. 32, no. 3, pp. 298–312, 2011.
- [23] D. Q. Mayne, “A Second-order Gradient Method for Determining Optimal Trajectories of Non-linear Discrete-time Systems,” *International Journal of Control*, vol. 3, pp. 85–95, 1966.
- [24] D. Q. Mayne and D. H. Jacobson, *Differential Dynamic Programming*. Springer Series in Operations Research and Financial Engineering, American Elsevier Publishing Company, 1970.
- [25] S. Yakowitz and B. Rutherford, “Computational aspects of discrete-time optimal control,” *Applied Mathematics and Computation*, vol. 15, no. 1, pp. 29–45, 1984.
- [26] L.-Z. Liao and C. Shoemaker, “Convergence in unconstrained discrete-time differential dynamic programming,” *IEEE Transactions on Automatic Control*, vol. 36, no. 6, pp. 692–706, 1991.
- [27] D. M. Murray and S. J. Yakowitz, “Differential dynamic programming and newton’s method for discrete time optimal control problems,” *Journal of Optimization Theory and Applications*, vol. 43, pp. 395–414, 1984.
- [28] W. Li and E. Todorov, “Iterative Linear Quadratic Regulator Design for Nonlinear Biological Movement Systems,” in *International Conference on Informatics in Control, Automation and Robotics (ICINCO)*, pp. 222–229, 2004.
- [29] M. Gifftthaler, M. Neunert, M. Stäuble, J. Buchli, and M. Diehl, “A family of iterative gauss-newton shooting methods for nonlinear optimal control,” in *IEEE/RSJ International Conference on Intelligent Robots and Systems (IROS)*, pp. 1–9, 2018.
- [30] T. A. Howell, B. E. Jackson, and Z. Manchester, “ALTRO: A Fast Solver for Constrained Trajectory Optimization,” in *IEEE/RSJ International Conference on Intelligent Robots and Systems (IROS)*, pp. 7674–7679, 2019.
- [31] Y. Aoyama, G. Boutselis, A. Patel, and E. A. Theodorou, “Constrained Differential Dynamic Programming Revisited,” in *IEEE International Conference on Robotics and Automation (ICRA)*, pp. 9738–9744, 2021.
- [32] Z. Xie, C. K. Liu, and K. Hauser, “Differential dynamic programming with nonlinear constraints,” in *IEEE International Conference on Robotics and Automation (ICRA)*, pp. 695–702, 2017.
- [33] R. Grandia, F. Farshidian, R. Ranftl, and M. Hutter, “Feedback MPC for Torque-Controlled Legged Robots,” in *IEEE/RSJ International Conference on Intelligent Robots and Systems (IROS)*, pp. 4730–4737, 2019.
- [34] S. Katayama and T. Ohtsuka, “Efficient solution method based on inverse dynamics for optimal control problems of rigid body systems,” in *IEEE International Conference on Robotics and Automation (ICRA)*, pp. 2070–2076, 2021.
- [35] Z. Manchester, N. Doshi, R. J. Wood, and S. Kuindersma, “Contact-implicit trajectory optimization using variational integrators,” *The International Journal of Robotics Research*, vol. 38, no. 12-13, pp. 1463–1476, 2019.
- [36] M. Posa, C. Cantu, and R. Tedrake, “A direct method for trajectory optimization of rigid bodies through contact,” *The International Journal of Robotics Research*, vol. 33, no. 1, pp. 69–81, 2014.
- [37] T. A. Howell, S. Le Cleac’h, S. Singh, P. Florence, Z. Manchester, and V. Sindhvani, “Trajectory Optimization with Optimization-Based Dynamics,” *IEEE Robotics and Automation Letters*, vol. 7, no. 3, pp. 6750–6757, 2022.
- [38] S. Le Cleac’h, T. A. Howell, S. Yang, C.-Y. Lee, J. Zhang, A. Bishop, M. Schwager, and Z. Manchester, “Fast Contact-Implicit Model Predictive Control,” *IEEE Transactions on Robotics*, vol. 40, pp. 1617–1629, 2024.
- [39] G. Kim, D. Kang, J.-H. Kim, S. Hong, and H.-W. Park, “Contact-implicit Model Predictive Control: Controlling diverse quadruped motions without pre-planned contact modes or trajectories,” *The International Journal of Robotics Research*, 2024.
- [40] W. Jallet, A. Bambade, N. Mansard, and J. Carpentier, “Constrained differential dynamic programming: A primal-dual augmented lagrangian approach,” in *IEEE/RSJ International Conference on Intelligent Robots and Systems (IROS)*, pp. 13371–13378, 2022.
- [41] J.-P. Sleiman, F. Farshidian, and M. Hutter, “Constraint Handling in Continuous-Time DDP-Based Model Predictive Control,” in *IEEE International Conference on Robotics and Automation (ICRA)*, pp. 8209–8215, 2021.
- [42] W. Jallet, A. Bambade, E. Arlaud, S. El-Kazdadi, N. Mansard, and J. Carpentier, “ProxDDP: Proximal Constrained Trajectory Optimization,” *IEEE Transactions on Robotics*, vol. 41, pp. 2605–2624, 2025.
- [43] A. Pavlov, I. Shames, and C. Manzie, “Interior Point Differential Dynamic Programming,” *IEEE Transactions on Control Systems Technology*, vol. 29, no. 6, pp. 2720–2727, 2021.
- [44] A. Wächter and L. Biegler, “On the implementation of an interior-point filter line-search algorithm for large-scale nonlinear programming,” *Mathematical Programming*, vol. 106, pp. 25–57, 2006.
- [45] L. Vanroye, A. Sathya, J. De Schutter, and W. Decré, “Fatrop: A fast constrained optimal control problem solver for robot trajectory optimization and control,” in *IEEE/RSJ International Conference on Intelligent Robots and Systems (IROS)*, pp. 10036–10043, IEEE, 2023.
- [46] D. M. Murray and S. J. Yakowitz, “Constrained differential dynamic programming and its application to multireservoir control,” *Water Resources Research*, vol. 15, no. 5, pp. 1017–1027, 1979.
- [47] S. Yakowitz, “The stagewise Kuhn-Tucker condition and

- differential dynamic programming,” *IEEE Transactions on Automatic Control*, vol. 31, no. 1, pp. 25–30, 1986.
- [48] Y. Tassa, N. Mansard, and E. Todorov, “Control-limited differential dynamic programming,” in *IEEE International Conference on Robotics and Automation (ICRA)*, pp. 1168–1175, 2014.
- [49] G. Lantoine and R. P. Russell, “A Hybrid Differential Dynamic Programming Algorithm for Constrained Optimal Control Problems. Part 1: Theory,” *Journal of Optimization Theory and Applications*, vol. 154, pp. 382–417, 2012.
- [50] Y. Aoyama, O. So, A. D. Saravanos, and E. A. Theodorou, “Second-Order Constrained Dynamic Optimization,” 2024.
- [51] S. Prabhu, S. Rangarajan, and M. Kothare, “Differential dynamic programming with stagewise equality and inequality constraints using interior point method,” 2024.
- [52] M. H. Wright, “Why a Pure Primal Newton Barrier Step May be Infeasible,” *SIAM Journal on Optimization*, vol. 5, no. 1, pp. 1–12, 1995.
- [53] J. Nocedal and S. J. Wright, *Numerical Optimization*. Springer Series in Operations Research and Financial Engineering, Springer, 2nd ed., 2006.
- [54] R. Bellman and R. Kalaba, *Dynamic Programming and Modern Control Theory*. Academic Press, Elsevier Science, 1965.
- [55] A. Wächter and L. T. Biegler, “Line Search Filter Methods for Nonlinear Programming: Motivation and Global Convergence,” *SIAM Journal on Optimization*, vol. 16, no. 1, pp. 1–31, 2005.
- [56] A. Wächter and L. T. Biegler, “Line Search Filter Methods for Nonlinear Programming: Local Convergence,” *SIAM Journal on Optimization*, vol. 16, no. 1, pp. 32–48, 2005.
- [57] R. H. Byrd, G. Liu, and J. Nocedal, “On the local behavior of an interior point method for nonlinear programming,” in *Numerical Analysis 1997* (D. F. Griffiths and D. J. Higham, eds.), pp. 37–56, Reading, MA, USA: Addison–Wesley Longman, 1997.
- [58] J. R. Bunch and L. Kaufman, “Some stable methods for calculating inertia and solving symmetric linear systems,” *Mathematics of Computation*, vol. 1, pp. 163–179, 1977.
- [59] G. Poole and L. Neal, “The rook’s pivoting strategy,” *Journal of Computational and Applied Mathematics*, vol. 123, no. 1, pp. 353–369, 2000. Numerical Analysis 2000. Vol. III: Linear Algebra.
- [60] J. A. E. Andersson, J. Gillis, G. Horn, J. B. Rawlings, and M. Diehl, “CasADi – A software framework for nonlinear optimization and optimal control,” *Mathematical Programming Computation*, vol. 11, no. 1, pp. 1–36, 2019.
- [61] M. Lubin, O. Dowson, J. Dias Garcia, J. Huchette, B. Legat, and J. P. Vielma, “JuMP 1.0: Recent improvements to a modeling language for mathematical optimization,” *Mathematical Programming Computation*, 2023.
- [62] M. N. Zeilinger, M. Morari, and C. N. Jones, “Soft Constrained Model Predictive Control With Robust Stability Guarantees,” *IEEE Transactions on Automatic Control*, vol. 59, no. 5, pp. 1190–1202, 2014.
- [63] J. Carpentier, G. Saurel, G. Buondonno, J. Mirabel, F. Lamiroux, O. Stasse, and N. Mansard, “The Pinocchio C++ library : A fast and flexible implementation of rigid body dynamics algorithms and their analytical derivatives,” in *IEEE/SICE International Symposium on System Integration (SII)*, pp. 614–619, 2019.
- [64] J. N. Nganga and P. M. Wensing, “Accelerating Second-Order Differential Dynamic Programming for Rigid-Body Systems,” *IEEE Robotics and Automation Letters*, vol. 6, no. 4, pp. 7659–7666, 2021.